Available online at www.sciencedirect.com
SCIENCE DIRECT
Journal of Sound and Vibration 296 (2006) 494–517
JOURNAL OF SOUND AND VIBRATION
www.elsevier.com/locate/jsvi

Analysis of the dispersion spectrum of fluid-loaded anisotropic plates: leaky-wave branches

A.L. Shuvalov*, O. Poncelet, M. Deschamps

Laboratoire de Mécanique Physique, Université Bordeaux 1, UMR CNRS 5469, 351, Cours de la Libération, F-33405 Talence Cedex, France

Received 1 June 2004; received in revised form 26 August 2005; accepted 14 December 2005
Available online 6 June 2006

Abstract

The supersonic complex-velocity versus real-frequency dispersion spectrum of the leaky waves in fluid-loaded anisotropic plates is discussed. Utilizing the sextic plate formalism provides approximate solutions for leaky-wave velocity in a form that reveals their basic features, such as the unique correspondence of the signs of its imaginary part and of the free-plate group velocity, the relation between the leakage and the rate of frequency dispersion, and the principal trends at low, high and near-cutoff frequencies in arbitrary anisotropic plates. A particular thrust of the study is the derivation of closed-form asymptotics for the fundamental leaky-wave velocity branch(es) at low frequency and for the continuum of leaky-wave branches near the fluid-coupled and fluid-uncoupled thickness resonances. Conditions for the asymptotics accuracy are analysed, and a comparison between an analytical approximation and exact numerical curves is presented for various cases.

1. Introduction

Many ultrasonic methods of studying immersed plates, such as reflection-transmission, acoustic microscopy and others, are intimately related to the leaky waves. These waves propagate along the plate at a phase velocity higher than the speed of sound c_f in the loading fluid (supersonic interval) and radiate energy into the fluid exterior. Various aspects of their properties have been explored in detail both experimentally and theoretically; see e.g. Refs. [1,2] for the ample references on this subject. The algebraic dispersion equation, underlying calculation of the leaky-wave spectrum, is well known and is an obvious starting point, but its exact solution is accessible only numerically. At the same time, an analytical perspective is indispensable for a unified understanding of the basic spectral trends, especially for arbitrarily anisotropic immersed plates. Analytical approximations also provide a benchmark for computer calculations, which tend to become more challenging with increasing anisotropy. Approximate solutions generally have to assume relatively light fluid loading and are obtained as a perturbation about the free-plate dispersion, which is also unknown explicitly; however, certain cases are capable of furnishing explicit asymptotics of the dispersion dependence directly in

*Corresponding author. Fax: +33 5 40006964.
E-mail address: a.shuvalov@lmp.u-bordeaux1.fr (A.L. Shuvalov).

0022-460X/$ - see front matter © 2006 Elsevier Ltd. All rights reserved.
doi:10.1016/j.jsv.2005.12.059

terms of material constants. The latter is significant for treating the inverse problem of material characterization.

The present study is concerned with an analytical treatment of the spectrum of leaky-wave complex velocity versus real frequency branches. These are understood in the conventional sense, as evolving from the real velocity branches of the free plate by way of acquiring a relatively small imaginary part and hence having the real part close to the free-plate velocity (although this restriction will be relaxed for some cases, particularly in the vicinity of thickness resonances). The treatment is based on the sextic plate formalism, which is particularly helpful for pursuing analytical results. By this means, firstly, the principal features of the leaky-wave dispersion in a fluid-loaded plate of unrestricted anisotropy are highlighted. Then their closed-form asymptotics at low and near-cutoff frequency are derived and analysed in detail.

It is noted that this paper follows up the paper [3], which has used the same theoretical framework for dealing with complex velocity branches in the subsonic interval (below c_f) of immersed-plate spectra.

2. Theoretical background

2.1. Sextic plate formalism

Consider an infinite anisotropic elastic plate with the density ρ and the elasticity tensor c_{ijkl}. Denote its thickness by $2h$ and the through-plate coordinate by y. Let $\mathbf{n}$ be the unit normal to the plate faces, and $\mathbf{m}$ be the unit vector parallel to the faces and is taken as the plane-wave propagation direction. The wavenumber k and trace velocity $v = \omega/k$ along $\mathbf{m}$ may be complex, whereas the frequency ω is assumed real and positive (unless otherwise specified). For future references, we will need the Stroh matrix

$$\mathbf{N}(v) = \begin{pmatrix} \mathbf{N}_1 & \mathbf{N}_2 \\ \mathbf{N}_3 - \rho v^2 \mathbf{I} & \mathbf{N}_1^{\mathrm{T}} \end{pmatrix}, \quad \begin{array}{l} \mathbf{N}_1 = -(nn)^{-1}(nm), \quad \mathbf{N}_2 = -(nn)^{-1}, \\ \mathbf{N}_3 = (mm) - (mn)(nn)^{-1}(nm), \end{array} \tag{1}$$

where $(ab) \equiv a_i c_{ijkl} b_l$ with $\mathbf{a}, \mathbf{b} = \mathbf{m}$ or $\mathbf{n}$; $\mathbf{I}$ is the identity matrix; T denotes transpose. Throughout the paper, whenever components c_{ijkl} appear explicitly, they are referred to the coordinate system X_1, X_2, X_3 with $X_1 \| \mathbf{m}$ and $X_2 \| \mathbf{n}$.

Basic concepts of the sextic plate formalism and its application to fluid-loaded plates [4,5] have already been introduced in the companion paper [3], so we will outline only some aspects, which are directly related to the problem at hand. The dispersion equation for a fluid-loaded plate (see below) involves the normal components of the 3×3 blocks of the plate admittance matrix $\mathbf{Y}$,

$$Y_1^{(\mathbf{n})} = \mathrm{i}\mathbf{n} \cdot \mathbf{M}_3^{-1}\mathbf{M}_1^{\mathrm{T}}\mathbf{n}, \quad Y_2^{(\mathbf{n})} = -\mathrm{i}\mathbf{n} \cdot \mathbf{M}_3^{-1}\mathbf{n}, \tag{2}$$

where $\mathbf{M}_1$ and $\mathbf{M}_3$ are the upper diagonal and the left off-diagonal blocks of the 6×6 propagator matrix $\mathbf{M} = \exp[2ikh\mathbf{N}(v)]$, relating the displacements and stresses at the plate faces. The condition of traction-free faces implies that $\det \mathbf{M}_3 = 0$, hence $Y_1^{(\mathbf{n})}$ and $Y_2^{(\mathbf{n})}$ are singular along the free-plate velocity branches, denoted by $\hat{v}_j(\omega)$ (j is the branch number). The singularity is the first-order pole in v, except the folding points on $\hat{v}_j(\omega)$, which are the second-order poles. The folding points are defined by the condition $\mathrm{d}\hat{v}_j/\mathrm{d}\omega \to \infty$ and hence imply that the in-plane component $\mathbf{g}_j \cdot \mathbf{m}$ of the group velocity $\mathbf{g}_j(\omega)$ turns to zero for a finite $\hat{v}_j$. Otherwise, near an arbitrary point $\hat{v}_j(\omega)$, for which $\mathbf{g}_j \cdot \mathbf{m} \neq 0$ and which is locally detached from other free-plate branches,

$$Y_1^{(\mathbf{n})}(v, \omega) \propto \frac{a_j(\omega)}{\rho\left[\hat{v}_j^2(\omega) - v^2\right]}, \tag{3}$$

whereas the singular part of $Y_2^{(\mathbf{n})}(v, \omega)$ for real v, ω differs from that of $Y_1^{(\mathbf{n})}$ only by a phase factor of a unit absolute value. Further analytical developments strongly hinge on the residue $a_j(\omega)$. It can be obtained in the form

$$a_j(\omega) = \frac{\rho \hat{v}_j^2 \omega |\hat{\mathbf{A}}_j \cdot \mathbf{n}|^2}{8h\langle K_j \rangle \mathbf{g}_j \cdot \mathbf{m}}, \tag{4}$$

where $\langle K_j\rangle = \frac{1}{2h}\int_{-h}^{h} K_j\,\mathrm{d}y$ with $K_j = \frac{1}{4}\rho\omega^2|\hat{\mathbf{A}}_j(y)|^2$ being the time-averaged kinetic energy in the plate with traction-free faces; $\hat{\mathbf{A}}_j(y)$ is the displacement at $v=\hat{v}_j(\omega)$; and $\hat{\mathbf{A}}_j$ is short for $\hat{\mathbf{A}}_j(\pm h)$, the displacement on either of the plate faces $y=\pm h$. By Eq. (4), a_j and $\mathbf{g}_j\cdot\mathbf{m}$ have the same signs:

$$\operatorname{sgn} a_j = \operatorname{sgn}\left(\mathbf{g}_j\cdot\mathbf{m}\right). \tag{5}$$

Using the identity [6]

$$\frac{\mathrm{d}\hat{v}_j}{\mathrm{d}\omega} = \frac{\omega\hat{\mathbf{A}}_j\cdot(\mathbf{N}_3-\rho\hat{v}_j^2\mathbf{I})\hat{\mathbf{A}}_j^*}{8\langle K_j\rangle\mathbf{g}_j\cdot\mathbf{m}} \tag{6}$$

(* denotes complex conjugate) allows re-writing the residue as

$$a_j(\omega) = \frac{\rho\hat{v}_j^2|\hat{\mathbf{A}}_j\cdot\mathbf{n}|^2}{\hat{\mathbf{A}}_j\cdot\left(\mathbf{N}_3-\rho\hat{v}_j^2\mathbf{I}\right)\hat{\mathbf{A}}_j^*}\frac{\mathrm{d}\hat{v}_j}{\mathrm{d}(\omega h)}. \tag{7}$$

2.2. Dispersion equation for leaky waves

Let the plate be immersed in a non-viscous fluid with the density ρ_f and speed of sound c_f. A fluid half-space admits two types of acoustic modes, one decreasing and one increasing into the fluid depth. Correspondingly, the dispersion equation for a fluid-loaded plate depends on the choice of modes in the fluids. The 'antisymmetric choice', which assumes the decreasing mode in one of the fluid half-spaces and the increasing mode in the other, leads in the supersonic interval to the equation for zeros of the reflection coefficient and is therefore irrelevant to the present context. The remaining options are associated with the 'symmetric choice', assuming that the modes in the both loading fluids are either decreasing or increasing. The corresponding forms of the dispersion equation are

$$\left[Y_1^{(\mathbf{n})}+\sqrt{Y_2^{(\mathbf{n})}Y_2^{(\mathbf{n})*}}-(\operatorname{sgn}v')Y_f\right]\left[Y_1^{(\mathbf{n})}-\sqrt{Y_2^{(\mathbf{n})}Y_2^{(\mathbf{n})*}}-(\operatorname{sgn}v')Y_f\right]=0 \tag{8}$$

for the choice of decreasing modes, and

$$\left[Y_1^{(\mathbf{n})}+\sqrt{Y_2^{(\mathbf{n})}Y_2^{(\mathbf{n})*}}+(\operatorname{sgn}v')Y_f\right]\left[Y_1^{(\mathbf{n})}-\sqrt{Y_2^{(\mathbf{n})}Y_2^{(\mathbf{n})*}}+(\operatorname{sgn}v')Y_f\right]=0, \tag{9}$$

for the choice of increasing modes. Here $Y_2^{(\mathbf{n})*}\equiv Y_2^{(\mathbf{n})*}(v,\omega)$ ($\neq[Y_2^{(\mathbf{n})}(v,\omega)]^*$ unless v,ω are real); $\operatorname{sgn}v'=\pm1$ for $v'\gtrless 0$; and

$$Y_f = -\mathrm{i}\frac{S^{(1)}(v)}{\rho_f v^2}, \tag{10}$$

where $S^{(1)}(v)$ is one of the Riemann sheets $S^{(n)}(v)$ ($n=1,2$) of the square root function $\sqrt{[(v^2/c_f^2)-1]}$, which are separated by the cut taken along the semi-axis $\operatorname{Im}\sqrt{v^2/c_f^2-1}=0$. By this definition, $S^{(1)}(v)=\pm\sqrt{\hat{v}_j^2/c_f^2-1}+\mathrm{i}0$ for $v=\hat{v}_j\pm\mathrm{i}0$ and $\hat{v}_j>c_f$.For more details, see Ref. [3].

Two methodological aspects are essential in specifying the dispersion equation for leaky waves in the vicinity of the free-plate branches $\hat{v}_j(\omega)$. First of them concerns the plate-related entries $Y_1^{(\mathbf{n})}+\sqrt{Y_2^{(\mathbf{n})}Y_2^{(\mathbf{n})*}}$ and $Y_1^{(\mathbf{n})}-\sqrt{Y_2^{(\mathbf{n})}Y_2^{(\mathbf{n})*}}$. Barring for the moment the special cases (they are addressed in Section 2.3), both $Y_1^{(\mathbf{n})}$ and $\sqrt{Y_2^{(\mathbf{n})}Y_2^{(\mathbf{n})*}}$ have the same residue at the first-order poles $\hat{v}_j$. The former term changes its sign on passing the pole, the latter does not. Hence, their adding and subtracting defines two locally different patterns, one diverging and the other smooth at $\hat{v}_j$. With reference to Eq. (3), denote the combination, diverging on both

sides of $\hat{v}_j$, by

$$\Phi_{\text{plate}}(v,\omega) \equiv Y_1^{(\mathbf{n})} \pm \sqrt{Y_2^{(\mathbf{n})} Y_2^{(\mathbf{n})*}} = \frac{2a_j(\omega)}{\rho\left[\hat{v}_j^2(\omega) - v^2\right]} + G(v,\omega) \tag{11}$$

($G(v,\omega)$ is a locally smooth function), where $\pm$ implies different signs on the opposite sides of $\hat{v}_j$: either $+$ for $v<\hat{v}_j$ and $-$ for $v>\hat{v}_j$ if $\mathbf{g}_j\cdot\mathbf{m}$ and hence a_j are positive; or vice versa if a_j and $\mathbf{g}_j\cdot\mathbf{m}$ are negative (see Eq. (5)). The inverse sign setting leads to the pattern with a smooth behaviour. The point is that only the diverging pattern (11) is relevant to seeking the leaky waves.

The second aspect concerns a choice of either increasing or decreasing modes in the loading fluids, see Eqs. (8) and (9). It is no longer optional once the dispersion equation is sought specifically in the form, which describes the leaky waves, i.e., admits the supersonic-velocity solutions $v_j(\omega) = v_j' + \mathrm{i}v_j''$ originating from the free-plate branches $\hat{v}_j(\omega)$. With such a premise, the 'correct' choice is unique (though not uniform across the spectrum): it prescribes taking the increasing fluid modes, if the in-plane group velocity $\mathbf{g}_j\cdot\mathbf{m}$ of the reference free-plate solution $\hat{v}_j(\omega)$ is positive, and the decreasing modes, if $\mathbf{g}_j\cdot\mathbf{m}$ is negative. Thus, the dispersion equation for leaky waves incorporates Eqs. (8) and (9) into the form

$$\Phi_{\text{plate}}(v,\omega) + (\operatorname{sgn} v')[\operatorname{sgn}(\mathbf{g}_j\cdot\mathbf{m})]Y_f = 0, \tag{12}$$

with $\Phi_{\text{plate}}(v,\omega)$ defined by Eq. (11). Eq. (12) provides a set of four reciprocally equivalent solutions $\pm\{v_j, v_j^*\}$, defining the waves with forward or backward direction of the phase-front propagation along $\mathbf{m}$ and with the energy flux directed away or towards the plate. Among these waves, the outflowing ones are the leaky waves. All four waves of the reciprocal set are either increasing or decreasing into the fluids, in agreement with the prerequisite setup fixed by the sign of $\mathbf{g}_j\cdot\mathbf{m}$. The alternative choice of fluid modes leads to the dispersion equation in the form, which has minus between the two terms of Eq. (12). Such equation simply does not admit solutions evolving from the free-plate velocity.[1] Properly fixing the fluid modes is important for both analytical and numerical treatment of leaky waves, based on whichever explicit approach (whether basing on the plate admittance and propagator or using decomposition into partial plate modes [1,2]).

The outlined leaky-wave setup can be verified on purely formal grounds. A complementary physical interpretation is, however, in order. It follows from the energy flux balance. For definiteness, consider the forward-propagating waves ($v'>0$). To the leading approximation in small v_j''/v_j',

$$P_{n,j}^{(f)} = 2k_j''h\langle\mathbf{P}_j\rangle\cdot\mathbf{m}, \tag{13}$$

where $k_j'' = \operatorname{Im}(\omega/v_j)$; $P_{n,j}^{(f)}$ is the normal component of the fluid-mode flux, which is taken at $\hat{v}_j$ on one of the fluid/plate interfaces and defined as being positive or negative when it is directed away or towards the plate, respectively; $\langle\mathbf{P}_j\rangle = \frac{1}{2h}\int_{-h}^{h}\mathbf{P}_j\,\mathrm{d}y$ with $\mathbf{P}_j = \mathbf{P}(\hat{v}_j)$ standing for the time-averaged flux in the free plate, so that [7]

$$\langle\mathbf{P}_j\rangle\cdot\mathbf{m} = 2\langle K_j\rangle\mathbf{g}_j\cdot\mathbf{m}. \tag{14}$$

Eqs. (13) and (14) confirm that for $\mathbf{g}_j\cdot\mathbf{m}>0$ the velocity v_j, having a negative imaginary part v_j'' and hence implying a decay along $\mathbf{m}$, corresponds to the leaky wave incorporating the outflowing fluid modes (with the flux away from the plate), i.e., to the leaky wave. The complex conjugated v_j^* corresponds to the wave growing along $\mathbf{m}$ due to the inflowing fluid modes (with the flux towards the plate). Both the outflowing and the inflowing modes, involved in this case, are increasing into the depth of the loading fluids (see Table 1 and Eqs. (8) and (9) in Ref. [3]). Choosing increasing fluid modes selects the dispersion equation in the form Eq. (9) and hence leads to Eq. (12). If, alternatively, $\mathbf{g}_j\cdot\mathbf{m}<0$, then by Eq. (13) the leaky wave with the outflowing fluid modes has $v_j''>0$ and hence decreases along the direction $-\mathbf{m}$ (inverse to phase-front propagation direction), whereas the wave with the inflowing fluid modes has $v_j''<0$ and so increases along $-\mathbf{m}$. In this case, both the outflowing and the inflowing fluid modes are decreasing, which means selecting the dispersion equation in the form (8) and thus also arriving at Eq. (12). Interestingly, on seeking a complex-frequency solution ω_j as a

[1] In the light of this, the more non-trivial is the fact that the free-plate flexural branch $\hat{v}_1$ gives rise to two immersed-plate branches (A and the A_0), satisfying two different dispersion equations associated with the alternative options of the symmetric choice of fluid modes [3]. The clue is real-valuedness of the A velocity branch confined to the subsonic range $v<c_f$.

function of real v ('temporal leakage', see Refs. [8,9]), the sign of its imaginary part ω_j'' induced by fluid loading is prescribed by the sign of $(\mathbf{g}_j \cdot \mathbf{m} - \hat{v}_j)$.

Eq. (12) may be further modified in order to yield only the forward-propagating leaky wave instead of four reciprocal solutions. Setting $v' > 0$ leaves us with two complex conjugated roots for inflowing and outflowing waves, and the leaky (outflowing) one is identified by the condition $\operatorname{sgn} v_j'' = -\operatorname{sgn}(\mathbf{g}_j \cdot \mathbf{m})$. Thus, recalling definition (10) of Y_f and, besides, inserting the local representation (11) of Φ_{plate} specifies Eq. (12) as follows:

$$\frac{2a_j(\omega)}{\rho\left[\hat{v}_j^2(\omega) - v^2\right]} + G(v,\omega) - \mathrm{i}\,[\operatorname{sgn}(\mathbf{g}_j \cdot \mathbf{m})]\frac{S^{(1)}(v)}{\rho_f v^2} = 0, \tag{15}$$

with

$$S^{(1)}(v) = -\sqrt{\hat{v}_j^2/c_f^2 - 1} + \mathrm{i}0 \quad \text{for } v = v' + \mathrm{i}v'' \to \hat{v}_j. \tag{16}$$

This formulation underlies the forthcoming analytical derivations for the leaky waves. It is noted that the case of a plate, which is fluid-loaded on one side and free on the other, is described by the same equations but with $\Phi_{\text{plate}} = Y_1^{(\mathbf{n})} = a_j/\rho(\hat{v}_j^2 - v^2) + G_1$ $(G_1 \neq G)$.

2.3. Perturbation-theory solution and the special cases

Assuming small v''/v' enables seeking an approximate solution of Eq. (15) for the leaky-wave velocity $v_j(\omega) = v_j' + \mathrm{i}v_j''$ with a relatively small imaginary part, which implies a weak leakage into the loading fluids in the sense of the energy flux relation (13) (whereas the absolute value of the displacement amplitudes in the fluid and the plate near their interface is generally of the same order, because their ratio contains the product of v_j''/v_j' and ρ/ρ_f). The leading-order solution of Eq. (15) for $v_j''(\omega)$ is

$$\frac{v_j''(\omega)}{\hat{v}_j(\omega)} = -\frac{\rho_f}{\rho}\frac{a_j}{\sqrt{\hat{v}_j^2/c_f^2 - 1}}. \tag{17}$$

It can also be obtained by combining Eqs. (4), (13) and (14) with the continuity of the normal displacements at the plate/fluid interfaces. The stipulation of small v_j''/v_j' is typically ensured by a small value of ρ_f/ρ or, sometimes, of a_j. By Eqs. (4) and (17), the sign of v_j'' is decided by that of $\mathbf{g}_j \cdot \mathbf{m}$, in agreement with Section 2.2.

Eq. (17) along with Eq. (7), expressing a_j via $\mathrm{d}\hat{v}_j/\mathrm{d}\omega$, illuminate the link between the 'dispersion rate' of a given free-plate branch $\hat{v}_j(\omega)$ and the leakage $v_j''(\omega)$, associated with this branch on fluid loading. The coefficient of proportionality between $v_j''(\omega)$ and $\mathrm{d}\hat{v}_j/\mathrm{d}\omega$ is usually a relatively slow function of ω. Thus the maximal leakage for the upper continuum of velocity branches and for the supersonic fundamental branch(es) corresponds to their steepest descend from the cutoffs for the former and from the low-frequency plateau for the latter (see comments to Figs. 1 and Fig. 3 below).

The approximate solution of Eq. (15) for the real part $v_j'(\omega)$ of the leaky-wave velocity is given by

$$\frac{v_j'(\omega) - \hat{v}_j(\omega)}{\hat{v}_j(\omega)} = \frac{1}{2}\left(\frac{\rho_f}{\rho}\right)^2 \frac{a_j^2}{\hat{v}_j^2/c_f^2 - 1}\left(\frac{2\rho\hat{v}_j^2 G_j}{a_j} - \frac{\hat{v}_j^2 - 3c_f^2}{\hat{v}_j^2 - c_f^2}\right), \tag{18}$$

where $G_j = G(\omega, \hat{v}_j)$. The difference between $v_j'(\omega)$ and the reference free-plate velocity $\hat{v}_j(\omega)$ is therefore small in the measure of $(\rho_f/\rho)^2$. Fluid-loading usually raises $v_j'(\omega)$ with respect to $\hat{v}_j(\omega)$ for the fundamental branches (see Section 3), however, their difference is not strictly sign-definite. A possibility of $v_j'(\omega) < \hat{v}_j(\omega)$ may be readily observed by appealing to the fluid-coupled thickness resonances, for which $\hat{v}_j^{-1} = 0$ while v_j' is finite.

Let us point out the special cases, violating or specifying the leaky-wave dispersion equation and its solutions (17) and (18). First, these solutions are certainly invalid near the point, at which the free-plate fundamental branch crosses the threshold c_f. This situation is considered in Section 3.1. The other special cases reside in 'the plate term' $\Phi_{\text{plate}}(v,\omega)$, see Eq. (11). A certain care is needed for dealing with the fundamental branches at high frequency. This is elaborated in Section 2.4. Near a folding point $\mathbf{g}_j \cdot \mathbf{m} = 0$, which breaks up a given free-plate branch $\hat{v}_j$ into two separate complex branches under fluid loading [10,11],

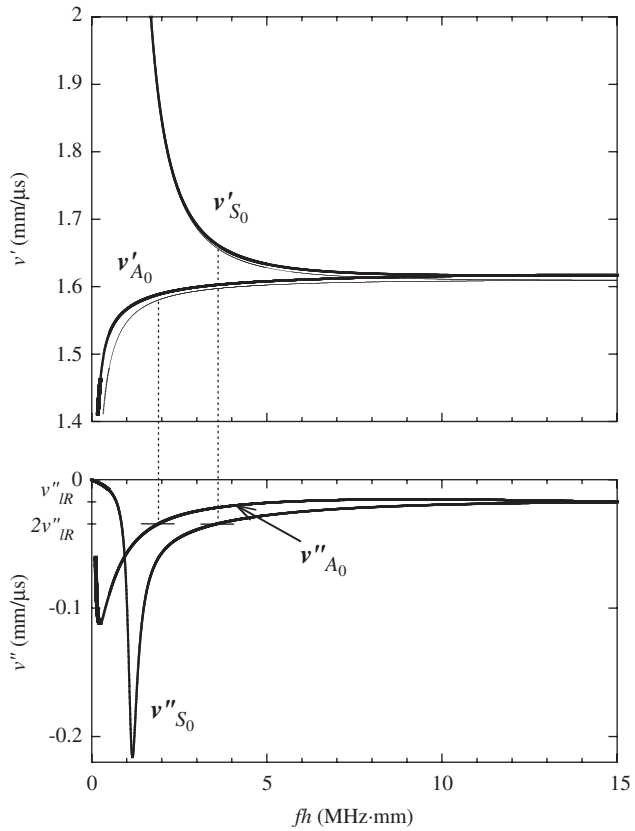

Fig. 1. The A_0 and S_0 velocity branches (bold lines), numerically calculated for the [1 1 0] propagation direction in a water-loaded (1 $\bar{1}$ 0)-cut copper plate. The level $2v''_{lR}$ is marked and related to the free-plate $A_0^{(\mathrm{free})}$ and $S_0^{(\mathrm{free})}$ branches (thin lines).

Eq. (11) is to be replaced by the expansion with respect to the second-order pole. Inserting this expansion into Eq. (12) reveals a locally increasing impact of fluid loading,

$$v_j''^2 \approx (v_j' - \hat{v}_j)^2 \sim \frac{\rho_f}{\rho}\hat{v}_j c_f. \tag{19}$$

If the reference pole is a point of intersection of two free-plate branches, Eq. (11) holds true but with a modified residue. If $\mathrm{d}\hat{v}_j/\mathrm{d}\omega = 0$ and hence $\hat{v}_j = \mathbf{g}_j \cdot \mathbf{m}$, which is when $\hat{\mathbf{A}}_j \cdot (\mathbf{N}_3 - \rho\hat{v}_j^2\mathbf{I})\hat{\mathbf{A}}_j^* = 0$ [6], the residue representation (4) remains valid, whereas its derivative form (7) is replaced by the expression through the second derivative $\mathrm{d}^2\hat{v}_j/\mathrm{d}\omega^2$. One more particular case is related to the points $\omega = \tilde{\omega}$ of fluid/plate uncoupling $\hat{\mathbf{A}}_j \cdot \mathbf{n} = 0$, at which $\hat{v}_j(\omega)$ and $v_j'(\omega)$ touch each other (see Ref. [5]). Near such points the factor $|\hat{\mathbf{A}}_j \cdot \mathbf{n}|^2$ in Eq. (4) and (7) is to be substituted by its perturbation proportional to $(\omega - \tilde{\omega})^2$. Note that the plate/fluid uncoupling is the only possibility for Eq. (12) to have the solutions $v_j' > c_f$ with zero imaginary part v_j''. Lastly, the treatment of leaky waves in the vicinity of the free-plate thickness resonances $\hat{v}_j^{-1}(\omega) = 0$ requires a modified approach, which is discussed in Section 4.

2.4. High-frequency trends of leakage

Assume hereafter that $c_f < v_R < v_L$, where v_R is the Rayleigh velocity and v_L is the so-called limiting velocity of the bulk-wave threshold [12] (the case $v_R < c_f$ is inspected in Ref. [3]). Generally, the free-plate branches $\hat{v}_j(\omega)$ at high ω tend to v_L, except for the two fundamental branches $\hat{v}_{1,2}(\omega)$, which tend to v_R. Both these limits imply waning frequency dispersion $\hat{v}_j(\omega) \to$ const., however, they yield different trends of the leakage $v_j''(\omega)$ under fluid loading.

Consider first the upper branches $\hat{v}_j(\omega)$. Typically their dispersion along the intermediate plateaus (transonic states) and along the bulk-wave threshold v_L is of the order of $(j/\omega)^2$ [13]. Hence, by Eqs. (7) and (17), the corresponding leakage $v''_j(\omega)$ caused by fluid loading tends to zero as $a_j(\omega)\sim\omega^{-3}$. Note that asymptotic nearing of the branches $\hat{v}_j(\omega)\to v_L$ is $\sim\omega^{-2}$, whereas the asymptotic formula (3) applies in the vicinity $|v-\hat{v}_j|\ll a_j/2\rho v_L\sim\omega^{-3}$ of each of these branches, so the consideration based on Eq. (3) remains valid. Interestingly, dealing with a complex frequency versus real velocity leads to the different conclusion: the imaginary part of frequency is not scaled by the dispersion derivative and hence the 'temporal leakage' ω''_j, associated with the upper branches under fluid loading, does not tend to zero with growing ω'_j.

The free-plate fundamental branches $\hat{v}_{1,2}(\omega)$ approach v_R with an exponentially weak frequency dependence. Hence, by Eq. (7), the numerator of the residues $a_{1,2}(\omega)$ decreases as $\mathrm{d}\hat{v}_j/\mathrm{d}\omega\sim\mathrm{e}^{-2\omega h/v_R}$. But the denominator of $a_{1,2}(\omega)$ also vanishes in the limit $\omega\to\infty$ (recall the identity $\hat{\mathbf{A}}_R\cdot(\mathbf{N}_3-\rho v_R^2\mathbf{I})\hat{\mathbf{A}}_R^*=0$ [14]); moreover, it can be shown to decrease with exactly the same rate as the numerator. This is why the residues $a_{1,2}(\omega)$ do not tend to zero and, via (17), yield a non-zero high-frequency limit of the leakage for A_0 and S_0 branches[2] evolving from $\hat{v}_{1,2}(\omega)$ under fluid loading. Indeed, this limit is nothing other than the imaginary part of the leaky Rayleigh-wave velocity v_{lR} for a fluid-loaded solid half-space: $v''_{A_0,S_0}(\omega)\to v''_{lR}$. The leading-order evaluation of v''_{lR} for isotropic solids goes back to Ref. [15]. For general anisotropy, the formalism developed in Ref. [16] readily yields

$$\frac{v''_{lR}}{v_R}=-\frac{\rho_f}{\rho}\frac{a_R}{2\sqrt{v_R^2/c_f^2-1}}, \tag{20}$$

with

$$a_R=-2\rho v_R\left[\frac{\mathrm{d}(1/Y_\infty^{(\mathbf{n})})}{\mathrm{d}v}\right]^{-1}_{v_R}=\frac{2\rho v_R|\hat{\mathbf{A}}_R\cdot\mathbf{n}|^2}{(-\mathrm{d}z_1/\mathrm{d}v)_{v_R}}. \tag{21}$$

Here $Y_\infty^{(\mathbf{n})}(v)=\mathbf{n}\cdot\mathbf{Z}_\infty^{-1}(v)\mathbf{n}$, and $\mathbf{Z}_\infty$ is the Lothe–Barnett 3×3 impedance matrix of the solid half-space [12]. It defines the Rayleigh wave by $\mathbf{Z}_\infty(v_R)\hat{\mathbf{A}}_R=\mathbf{0}$, and $z_1(v)$ in Eq. (21) is that one of its eigenvalues (real, single and decreasing for $v<v_L$) which turns to zero at v_R. Explicit evaluation of $\mathbf{Z}_\infty$ for anisotropic solids can be handled by various methods, see e.g. Refs. [12,14,17]. Note that in many typical cases v_R is fairly close to v_L, and then the leakage v''_{lR} acquires a small numerical factor because of large $(-\mathrm{d}z_1/\mathrm{d}v)_{v_R}\propto(v_L-v_R)^{-1/2}$. The case of 'double leakage' into both the fluid and the (anisotropic) solid half-spaces, which is stipulated by the Rayleigh wave with $v_R>v_L$, has been studied in Ref. [18].

It is instructive to compare Eqs. (17) and (20). Generally, by Eqs. (11) and (12), a pole at $\hat{v}_j$ affects v''_j with the 'force' proportional to $2a_j$, which accounts for the equal contributions of $Y_1^{(\mathbf{n})}$ and $\sqrt{Y_2^{(\mathbf{n})}Y_2^{(\mathbf{n})*}}$. Now consider $\omega\to\infty$ and $v<v_L$. Then $Y_1^{(\mathbf{n})}(v,\omega)\to Y_\infty^{(\mathbf{n})}(v)$ and so its residues $a_{1,2}(\omega)$ referred, respectively, to $\hat{v}_{1,2}(\omega)$ tend to a_R; but at the same time $Y_2^{(\mathbf{n})}(v,\omega)\to 0$ for $v\neq v_R$. It is also noted that asymptotical nearing of the branches (poles) $\hat{v}_{1,2}(\omega)\to v_R$ leads to merging rather than adding their contributions, for, $\mathbf{Z}_\infty$ has a single zero at v_R. Thus, the Rayleigh pole v_R affects v''_{lR} with the 'force' proportional to a_R, instead of $2a_j$ in Eq. (11). This is the reason for the additional factor $\frac{1}{2}$ acquired by v''_{A_0} and v''_{S_0} in their high-frequency limit (20) comparatively to Eq. (17). This effect of a 'weakening' pole modifies appropriately Eqs. (11), (17) and (18), when these are used for the A_0 and S_0 branches at high frequency. The same point is evident on invoking the case of one-sided fluid loading (see the remark below (15)): for low and intermediate frequency, the leakage $v''_{1,2}(\omega)$ is approximately twice less than for the two-sided loading, but the high-frequency limit v''_{lR} of $v''_{A_0}(\omega)$ and $v''_{S_0}(\omega)$ for both two-sided and one-sided loading is certainly identical.

[2]The conventional notations A_0 and S_0 (or v_{A_0} and v_{S_0}) are actually related to the assumption of a symmetry plane parallel to the plate faces, however, we shall follow Ref. [3] in using them as well for the case of arbitrary anisotropy. For the reference branches in a free plate, the notations $\hat{v}_1$, $\hat{v}_2$ will be used alongside $A_0^{(\mathrm{free})}$ and $S_0^{(\mathrm{free})}$ (or $\hat{v}_{A_0}$ and $\hat{v}_{S_0}$).

3. Fundamental leaky branches

3.1. A_0 branch

We continue with the case $c_f < v_R$, so that $\hat{v}_1(\omega)$ (the free-plate flexural $A_0^{(\mathrm{free})}$ branch) and the real part $v'_{A_0}(\omega)$ of the A_0 branch cross the c_f level. The subsonic behaviour of this branch and, in particular, the condition for existence of the A_0 loop of purely real solutions have been examined in Ref. [3]. A strong impact of fluid loading, characterizing transformation of $A_0^{(\mathrm{free})}$ to A_0 branch in the subsonic domain, is taken over by a comparatively weaker effect in the supersonic velocity interval. This two different trends adjust to each other in the intermediate range $|\hat{v}_1^2/c_f^2 - 1|^{1/2} \lesssim \rho_f/\rho$, which is where $\hat{v}_1(\omega)$ and $v'_{A_0}(\omega)$ cross the c_f-level. Here 'the supersonic' equations (17) and (18) are not valid yet; instead, v_{A_0} may be locally estimated by

$$v'_{A_0} - \hat{v}_1 = C_{\mathrm{r}} c_f \left(\frac{\rho_f}{\rho} a_1\right)^{2/3}, \quad v''_{A_0} = -C_{\mathrm{i}} c_f \left(\frac{\rho_f}{\rho} a_1\right)^{2/3}, \tag{22}$$

with the coefficients C_{r} markedly smaller than 1 and C_{i} of the order of 1 (note that the subsonic A branch, arising from $A_0^{(\mathrm{free})}$ due to decreasing fluid modes, departs downwards from $\hat{v}_1(\omega) \sim c_f$ in the same measure of $(\rho_f/\rho)^{2/3}$). With further growing ω and hence the fluid impact falling off, Eq. (22) is superseded by Eqs. (17) and (18).

An overall shape of the curves $v'_{A_0}(\omega)$ and $v''_{A_0}(\omega)$ largely depends on the presence or absence of the real subsonic loop. If it exists, then the curve $v''_{A_0}(\omega)$ has a maximum on both sides of the frequency interval $v''_{A_0}(\omega) = 0$ of the real loop existence. With ρ_f/ρ taken as a continuously growing variable, the loop shrinks and then disappears; correspondingly, the two maxima of $v''_{A_0}(\omega)$ approach each other and then merge into a single extremum, associated with the region of strongest dispersion along the $A_0^{(\mathrm{free})}$ branch (see Fig. 7 in Ref. [3]).

Another general feature of the A_0-branch leakage has to do with its high-frequency adjustment from Eqs. (17) to (20) (see Section 2.4). The $A_0^{(\mathrm{free})}$ branch $\hat{v}_1(\omega)$ commonly reaches an essentially flat plateau when the frequency is not very high and so $v''_{A_0}(\omega)$ may be described by Eq. (17). A waning dispersion of the velocity $\hat{v}_1(\omega) \to v_R$ with further growing frequency entails small variation of $a_1(\omega)$ on its tendency to a_R. At the same time, the leakage $v''_{A_0}(\omega)$ decreases approximately by half from its value (17) at the beginning of the Rayleigh shoulder to the high-frequency limit v''_{lR} given by Eq. (20). A similar trend pertains to the upper fundamental branch S_0, although in a less conspicuous fashion, because flattening along the Rayleigh shoulder becomes prominent for the $S_0^{(\mathrm{free})}$ branch usually from a higher frequency than for $A_0^{(\mathrm{free})}$.

The outlined observations are exemplified for the [1 1 0] propagation in a water-loaded $(1\,\bar{1}\,0)$-cut copper plate in Fig. 1. The density of copper is $\rho = 8.932\,\mathrm{g/cm^3}$ and the elastic coefficients in the basis with $X_1 \| [1\,1\,0]$ and $X_2 \| [1\,\bar{1}\,0]$ (see Section 2.1) are $c_{11} = c_{22} = 222$, $c_{33} = 170$, $c_{12} = 71$, $c_{13} = c_{23} = 123$, $c_{44} = c_{55} = 75.5$, $c_{66} = 23.5\,\mathrm{GPa}$.

In conclusion, let us address a possibility of evaluating the supersonic extent of the A_0 branch by means of the low-frequency approximation. The necessary condition is that the free-plate branch $A_0^{(\mathrm{free})}$ crosses c_f at a frequency low enough to admit such approximation. The low-frequency asymptotics for the $A_0^{(\mathrm{free})}$ branch, truncated by the leading order, read

$$\hat{v}_1(\omega) = \sqrt{2\kappa\omega h}, \quad a_1(\omega) = \sqrt{\frac{\kappa}{8\omega h}}, \tag{23}$$

where $\kappa = \sqrt{(1/12\rho)\mathbf{m}\cdot\mathbf{N}_3\mathbf{m}}$ ($\mathbf{N}_3$ is the Stroh-matrix block, see Eq. (1)). Taking $\hat{v}_1 = c_f$ with $\hat{v}_1 = 2\kappa kh$ and demanding $2kh(= 2\omega h/\hat{v}_1) \ll 1$ yields the sought condition in the form

$$c_f \ll \kappa. \tag{24}$$

This strong inequality is certainly not applicable to typical plate materials and loading fluids, for which the $A_0^{(\mathrm{free})}$ branch crosses c_f far beyond the low-frequency range. It is, however, feasible if c_f stands for the speed of sound in gas. In the case of gas loading, the low-frequency estimate can still be used in Eq. (17) for approximating a certain supersonic range of the A_0 branch as long as $2\omega h/\hat{v}_1 \ll 1$ (with actual $\hat{v}_1(\omega)$) remains valid. Fig. 2, plotted for a copper plate ($\kappa \approx 2.73\,\mathrm{mm/\mu s}$) loaded by air ($\rho_f = 0.0012\,\mathrm{g/cm^3}$, $c_f = 0.34\,\mathrm{mm/\mu s}$),

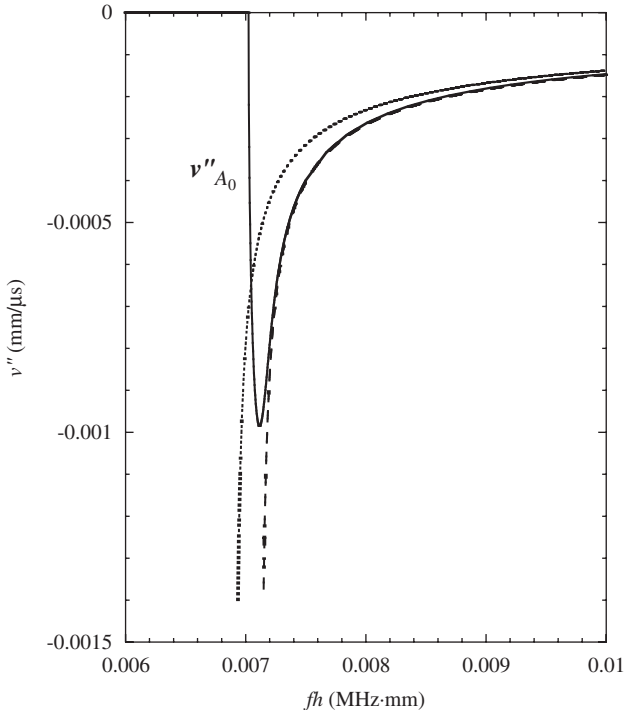

Fig. 2. The imaginary part $v''_{A_0}(\omega)$ of the A_0 branch for the [1 1 0] propagation direction in a $(1\ \bar{1}\ 0)$-cut copper plate loaded by air. Solid line is the exact calculation; dashed line is the approximation, which starts from estimate (22) (with $a_1 = \kappa/2c_f$; $C_i = 1$) and is continued by Eq. (17) with $a_1(\omega) = \sqrt{\kappa/8\omega h}$ and with exact data for $\hat{v}_1(\omega)$ in the denominator; dotted line is the same approximation but with $\hat{v}_1(\omega) = \sqrt{2\kappa\omega h}$.

demonstrates a comparison between the exact curve $v''_{A_0}(\omega)$ and its explicit approximation via Eq. (17) with Eq. (23). Regarding the subsonic part of the A_0 branch, we recall that under air loading it is dominated by the broad real-valued loop, see Ref. [3].

3.2. The low-frequency asymptotics for the upper fundamental branches

For low ω, the leading-order frequency dependence of the velocity and displacement vector for the two upper fundamental branches in a free plate is

$$\hat{v}_j(\omega) = \hat{v}_j^{(0)}\left[1 - \widehat{B}_j\left(\frac{\omega h}{\hat{v}_j^{(0)}}\right)^2\right], \quad \hat{\mathbf{A}}_j(y) = U_j\left[\mathbf{e}_j + \frac{\mathrm{i}\omega}{\hat{v}_j^{(0)}}(y\mathbf{I} + h\mathbf{e}_j \otimes \mathbf{e}_j)\mathbf{N}_1\mathbf{e}_j\right], \quad j = 2, 3, \tag{25}$$

where U_j is a disposable normalization constant and the plate faces are located at $y = \pm h$. The values $\hat{v}_j^{(0)}$ and $\mathbf{e}_j$, referred to the limit $\omega \to 0$, are defined by the eigenspectrum of $\mathbf{N}_3$:

$$\left(\mathbf{N}_3 - \rho\hat{v}_j^{(0)2}\mathbf{I}\right)\mathbf{e}_j = \mathbf{0}, \ \mathbf{e}_j \cdot \mathbf{n} = 0, \quad j = 2, 3 \tag{26}$$

and

$$\widehat{B}_j = -\frac{1}{6\rho\hat{v}_j^{(0)2}}\mathbf{e}_j \cdot \mathbf{N}_1^{\mathrm{T}}\left(\mathbf{N}_3 - \rho\hat{v}_j^{(0)2}\mathbf{I}\right)\mathbf{N}_1\mathbf{e}_j, \quad j = 2, 3. \tag{27}$$

In the case of generic anisotropy both these branches are dispersive, and the onset for the lower of $\hat{v}_2(\omega)$, $\hat{v}_3(\omega)$ may be either decreasing or increasing whereas that for the higher branch is always decreasing. The coefficients

of asymptotics simplify in the presence of a symmetry plane m. For instance, if the plate faces are parallel to a symmetry plane m, then $\widehat{B}_j = \frac{1}{6}(\mathbf{n}\cdot\mathbf{N}_1\mathbf{e}_j)^2$, $j=2,3$. If m coincides with the sagittal plane $(\mathbf{m},\mathbf{n})$, so that one of the branches $\hat{v}_{2,3}(\omega)$ is the SH non-dispersive branch, then the onset of the other branch, starting off either above or below the SH-wave velocity, has the coefficient $\widehat{B}_j = \frac{1}{6}(\mathbf{n}\cdot\mathbf{N}_1\mathbf{m})^2$ (see details in Refs. [4,19]).

Assume the typical case, when the least of $\hat{v}_j^{(0)}$ exceeds c_f of the loading fluid and so both (dispersive) fundamental branches $v_j(\omega)$ in the immersed plate are complex off the zero frequency limit. Consider their low-frequency approximation. Utilizing Eq. (7) with Eqs. (25) and (26) gives

$$a_j(\omega) = \frac{\omega h}{2\hat{v}_j^{(0)}}(\mathbf{n}\cdot\mathbf{N}_1\mathbf{e}_j)^2, \quad j=2,3. \tag{28}$$

Inserting this into Eq. (17) yields the leading-order estimate of the leakage,

$$v_j''(\omega) = -\frac{\rho_f}{\rho}\omega h\frac{(\mathbf{n}\cdot\mathbf{N}_1\mathbf{e}_j)^2}{2\sqrt{\hat{v}_j^{(0)2}/c_f^2-1}}, \quad j=2,3. \tag{29}$$

Eq. (29) evaluates the linear slope of $v_j''(\omega)$ for any ρ_f/ρ, not necessarily small. This is due to proportionality of the residues $a_j(\omega)$ to $\omega h/\hat{v}_j^{(0)} \ll 1$ (by contrast to the case of the flexural branch), so that the aggregate small parameter is a product of ρ_f/ρ and $\omega h/\hat{v}_j^{(0)}$. Moreover, the quantity $\mathbf{n}\cdot\mathbf{N}_1\mathbf{e}_j$, which is of the order of ratio of the non-diagonal to diagonal elasticity coefficients c_{IJ}, usually entails an additional numerical smallness reducing the initial slope of $v_j''(\omega)$. Note that if neither the plane of plate faces nor the sagittal plane coincide with a symmetry plane whereas the propagation direction $\mathbf{m}$ is orthogonal to a symmetry plane, then the residue for the quasi-SH wave is of the order of $(\omega h)^3$, and therefore so is this wave leakage.

Substituting Eq. (28) along with evaluated $G_j \sim \omega h/\hat{v}_j^{(0)}$ (see Ref. [5]) into Eq. (18) gives the leading-order asymptotics for the real part in the form

$$v_j'(\omega) = \hat{v}_j(\omega)\left[1+\left(\frac{\rho_f}{\rho}\right)^2 B_j\left(\frac{\omega h}{\hat{v}_j^{(0)}}\right)^2\right] \approx \hat{v}_j^{(0)}\left\{1-\left[\widehat{B}_j-\left(\frac{\rho_f}{\rho}\right)^2 B_j\right]\left(\frac{\omega h}{\hat{v}_j^{(0)}}\right)^2\right\}, \tag{30}$$

with

$$B_j = \frac{(\mathbf{n}\cdot\mathbf{N}_1\mathbf{e}_j)^2}{2\left(\hat{v}_j^{(0)2}/c_f^2-1\right)}\left[\frac{(\mathbf{n}\cdot\mathbf{N}_1\mathbf{e}_k)^2}{\hat{v}_k^{(0)2}/\hat{v}_j^{(0)2}-1} - \rho\hat{v}_j^{(0)2}\mathbf{n}\cdot\mathbf{N}_2\mathbf{n} + \frac{\hat{v}_j^{(0)2}+c_f^2}{4\left(\hat{v}_j^{(0)2}-c_f^2\right)}(\mathbf{n}\cdot\mathbf{N}_1\mathbf{e}_j)^2\right], \quad j,k=2,3,\ k\neq j. \tag{31}$$

By Eq. (31), in which $\mathbf{N}_2$ is negative definite (see Eq. (1)), a positive value of B_j is ensured for the lower of two (dispersive) fundamental branches $v_j'(\omega)$, so that its low-frequency onset is always higher than in the free plate,

$$v_j'(\omega) > \hat{v}_j(\omega) \tag{32}$$

and this is also true as a rule for the higher branch. In the presence of the SH non-dispersive and fluid-uncoupled branch $v_j = \hat{v}_{\mathrm{SH}}$ ($\mathbf{n}\cdot\mathbf{N}_1\mathbf{e}_j = 0$ for $\mathbf{e}_j = \mathbf{m}\times\mathbf{n}$), the other branch always has $B_j > 0$. Thus, the overall conclusion is that typically the coefficients $\widehat{B}_j$ and B_j are positive. Assuming this hereafter, it is seen from Eq. (30) that the low-frequency trend of $v_j'(\omega)$ is described by the two competitive factors: the free-plate dispersion proportional to $\widehat{B}_j$ drives the curve $v_j'(\omega)$ downward, whereas the 'fluid-induced' dispersion proportional to $(\rho_f/\rho)^2 B_j$ forces it upward. As a result,

$$v_j'(\omega) < \hat{v}_j^{(0)} \quad \text{for} \quad (\rho_f/\rho)^2 B_j < \widehat{B}_j, \quad v_j'(\omega) > \hat{v}_j^{(0)} \quad \text{for} \quad (\rho_f/\rho)^2 B_j > \widehat{B}_j. \tag{33}$$

It is obvious indeed that the low-frequency onset of $v_j'(\omega)$ bends downward alongside $\hat{v}_j(\omega)$ if ρ_f/ρ is small; what is interesting is that $v_j'(\omega)$ goes upward if ρ_f/ρ is large enough (recall to this end that asymptotics (30) does not require the assumption of small ρ_f/ρ).

As an example, consider the S_0 leaky fundamental branch in an immersed plate with the faces and the sagittal plane $(\mathbf{m},\mathbf{n})$ parallel to the symmetry planes. Hereafter in this subsection, the branch label $j = S_0$ is

adopted. With $X_1 \| \mathbf{m}$ and $X_2 \| \mathbf{n}$, Eq. (29) specifies as

$$v''_{S_0}(\omega) = -\frac{\rho_f}{\rho}\omega h \frac{c_{12}^2/c_{22}^2}{2\sqrt{\hat{v}_{S_0}^{(0)\,2}/c_f^2 - 1}} \tag{34}$$

and Eq. (30) holds with $\hat{v}_{S_0}^{(0)2} = 12\kappa^2 = \frac{1}{\rho}(c_{11} - c_{12}^2/c_{22})$ and

$$\widehat{B}_{S_0} = \frac{1}{6}\frac{c_{12}^2}{c_{22}^2}, \quad B_{S_0} = \frac{c_{12}^2/c_{22}^2}{8\left(\hat{v}_{S_0}^{(0)\,2}/c_f^2 - 1\right)}\left(4\frac{c_{11}}{c_{22}} - 3\frac{c_{12}^2}{c_{22}^2} + \frac{2c_{12}^2/c_{22}^2}{\hat{v}_{S_0}^{(0)\,2}/c_f^2 - 1}\right), \tag{35}$$

where $B_{S_0} > 0$. To improve the approximation accuracy, the asymptotics $(25)_1$ for the $S_0^{(\mathrm{free})}$ branch will be complemented by the next-order asymptotics

$$\hat{v}_{S_0}^2(\omega) = \hat{v}_{S_0}^{(0)2}\left[1 - \frac{1}{3}\frac{c_{12}^2}{c_{22}^2}\left(\frac{\omega h}{\hat{v}_{S_0}^{(0)}}\right)^2 - \frac{2}{15}\frac{c_{12}^2}{c_{22}^2}\left(\frac{c_{11}}{c_{22}} + \frac{1}{3}\frac{c_{12}}{c_{22}} - \frac{c_{12}^2}{c_{22}^2}\right)\left(\frac{\omega h}{\hat{v}_{S_0}^{(0)}}\right)^4\right]. \tag{36}$$

Fig. 3 shows a comparison between the exact calculation and the low-frequency approximations for the S_0 branch in water-loaded plates of copper and Plexiglas ($\rho = 1.18\,\mathrm{g/cm^3}$; $c_{11} = 7.375$, $c_{12} = 3.977\,\mathrm{GPa}$). The leading-order asymptotics (34), which identifies only the linear slope of leakage $v''_{S_0}(\omega)$, may be complemented by an estimate of the frequency of $v''_{S_0}(\omega)$ extremum, assuming that the latter occurs near the steepest descend of the free-plate branch $\hat{v}_{S_0}(\omega)$. For the plate materials at hand, the extremes of $\mathrm{d}\hat{v}_{S_0}/\mathrm{d}\omega$ and of v''_{S_0} are located, respectively, at $fh \approx 1.15$ and $1.17\,\mathrm{MHz\,mm}$ for copper (see Fig. 1) and at $fh \approx 0.45$ and $0.52\,\mathrm{MHz\,mm}$ for Plexiglas (see Fig. 3b). These values are in a good agreement with Eq. (17) incorporating Eq. (7). Consider now the real part of the S_0 branch. For the copper plate ($\rho_f/\rho \ll 1$), the curve $v'_{S_0}(\omega)$ is very close

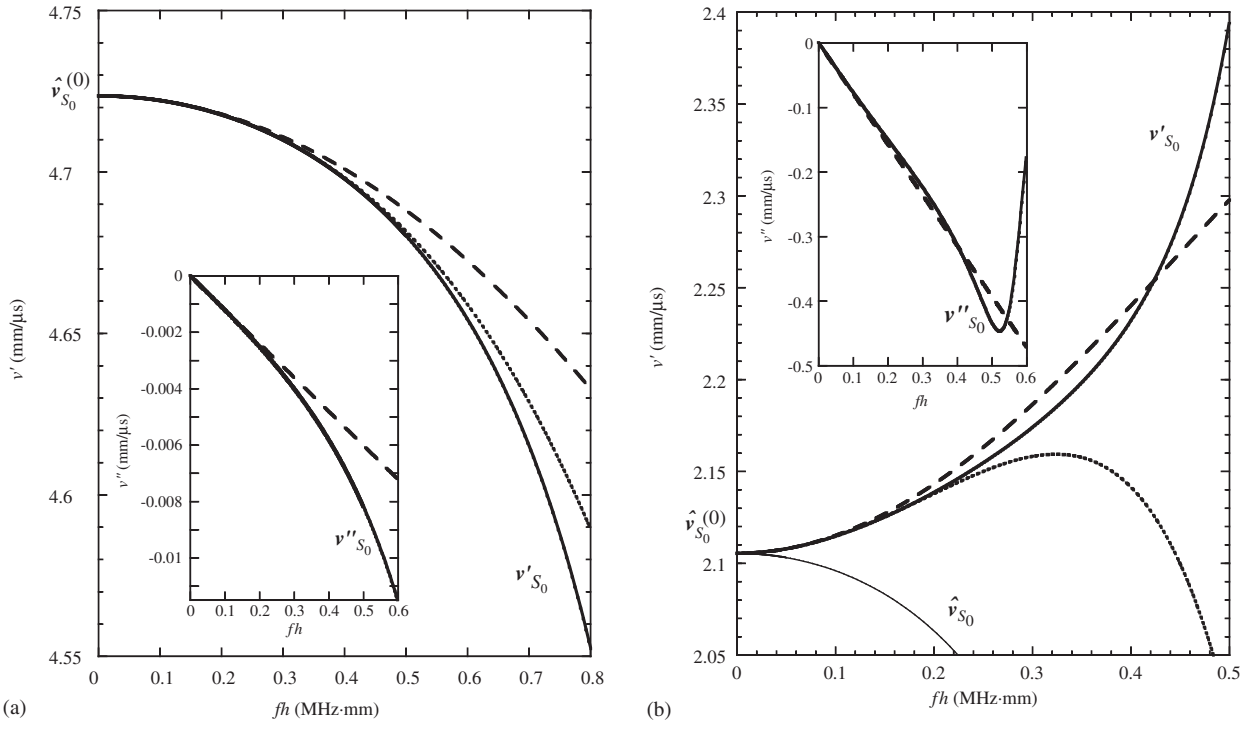

Fig. 3. Low-frequency onset of the S_0 branch: (a) for the [1 1 0] propagation direction in a water-loaded $(1\,\bar{1}\,0)$-cut copper plate; (b) for a water-loaded Plexiglas plate. Solid lines represent the exactly calculated real and imaginary parts $v'_{S_0}(\omega)$, $v''_{S_0}(\omega)$. Dashed lines show the leading-order asymptotics of $v'_{S_0}(\omega)$, given by Eq. (30) with Eq. (35), and of $v''_{S_0}(\omega)$, given by Eq. (34); the dotted line is the asymptotics for $v'_{S_0}(\omega)$, given by Eq. (30) with Eq. (36). Thin line in (b) is the free-plate branch $\hat{v}_{S_0}(\omega)$, added for comparison.

to the free-plate branch $\hat{v}_{S_0}(\omega)$: their difference is less than 10^{-3} mm/μs at $fh = 0.5$ MHz mm (too small to separate these curves in Fig. 3a). On the other hand, a relatively large value of ρ_f/ρ in the case of a Plexiglas plate entails the curve $v'_{S_0}(\omega)$, which differs drastically from the free-plate branch $\hat{v}_{S_0}(\omega)$ and folds upward in accord with Eq. (33), see Fig. 3b.

The case of a relatively large ρ_f/ρ is fairly often encountered in practical applications, e.g., it is typical for many types of light composites. In this regard, it is interesting to explore the evolution of the low-frequency onset of $v'_{S_0}(\omega)$ from descending to ascending pattern with growing density ratio ρ_f/ρ. (Similar phenomena due to internal absorption in unloaded plates has been discussed in Refs. [20–22].) Corresponding simulation is presented in Fig. 4. Its qualitative interpretation is as follows. At small ρ_f/ρ the branch $v'_{S_0}(\omega)$ is close to steadily descending free plate branch $S_0^{(\mathrm{free})}$ (the bold curve 1 in Fig. 4). The effect of growing ρ_f/ρ, which is at first more prominent for low frequency, flattens the initial trend of $v'_{S_0}(\omega)$ and hence makes its subsequent descend steeper. This causes a decrease of the average (integrated across the plate) horizontal energy flux, related to this part of the dispersion curve. As ρ_f/ρ continues to increase, the flux becomes too small to remain compatible with the wave-field distribution pertaining to the S_0 branch, and so $v'_{S_0}(\omega)$ has to jump onto the 'trajectory' of the real part of the S_1 branch. Hence, for a certain value of density ratio, denoted, say, by $(\rho_f/\rho)_c$, both the real and imaginary parts of the immersed-plate branches $v_{S_0}(\omega)$ and $v_{S_1}(\omega)$ must intersect at the same frequency ω_{int} (see the curves 2 in Fig. 4). With further growing $\rho_f/\rho > (\rho_f/\rho)_c$, the branches $v_{S_0}(\omega)$ and $v_{S_1}(\omega)$ break apart (the curves 3 in Fig. 4). The low-frequency part $v'_{S_0}(\omega)$, approximated by Eq. (30),

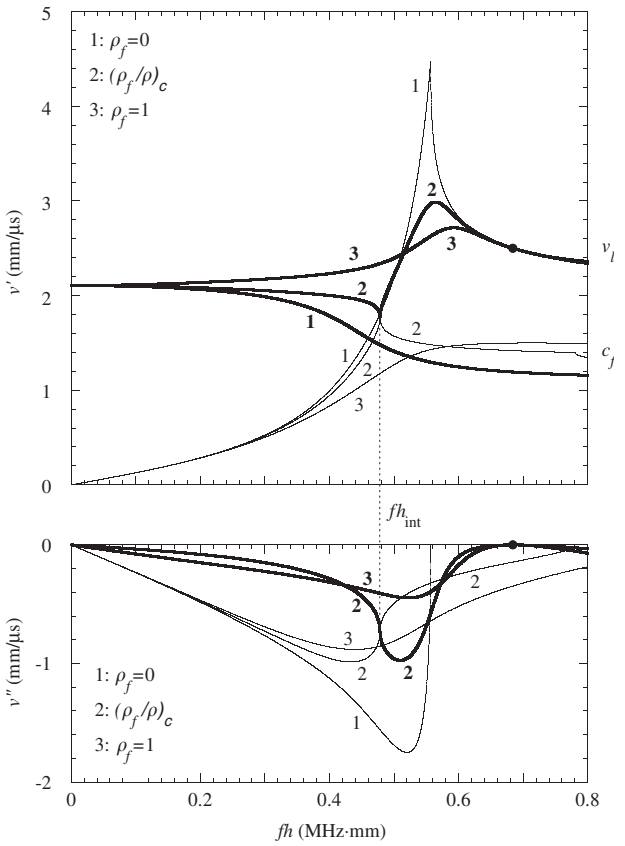

Fig. 4. Simulation of low-frequency evolution of the S_0 branch in a Plexiglas plate with growing density of the loading fluid ($c_f = 1.5$ mm/μs). The two curves 1 are the free-plate branches $S_0^{(\mathrm{free})}$ (bold line) and $S_1^{(\mathrm{free})}$ (thin line for both the complex-valued segment, running from the folding point to $\omega = 0$, and for the continuation of the real branch). The curves 2 correspond to the critical value $(\rho_f/\rho)_c$, which entails intersection of the complex branches S_0, S_1 and triggers their changeover. The curves 3, representing S_0 (bold line) and S_1 (thin line) after the changeover, are plotted for water loading. The filled circle indicates the point of plate/fluid uncoupling at $v = v_l$ and $\omega = \pi/h\sqrt{v_t^{-2} - v_l^{-2}}$. Note that a kink on the curve 2 slightly below $v = c_f$ pinpoints the opening of real-valued arch (cf. Fig. 9 in Ref. [3]).

raises upward in order to adjust to the 'new' trajectory on the right-hand side of $\omega_{\rm int}$, where the same leaky-wave branch is no longer topologically related to the $S_0^{(\rm free)}$ branch but rather to the non-propagating $S_1^{(\rm free)}$ branch of the free plate. Note that the value $(\rho_f/\rho)_c$, which triggers $S_0 \to S_1$ changeover, is slightly less than another reference value $(\rho_f/\rho)_0$, for which the onset of $v'_{S_0}(\omega)$ becomes horizontal. Thus, with reference to Eqs. (30) and (33),

$$(\rho_f/\rho)_c \lesssim (\rho_f/\rho)_0 = \sqrt{\widehat{B}_{S_0}/B_{S_0}}. \tag{37}$$

For the case of Plexiglas, $(\rho_f/\rho)_c = 0.37$ and $(\rho_f/\rho)_0 = 0.59$.

Fig. 4 demonstrates in passing a noteworthy general property: for the symmetrical branches $\hat{v}_{S_n}(\omega)$ $(n = 1, 2, \ldots)$ of a free plate, the wave field does not penetrate into an *arbitrary* adjoined fluid (plate/fluid uncoupling, see Section 2.3) at the points, where $\hat{v}_{S_n}(\omega)$ meet the velocity v_l of the pure longitudinal bulk wave propagating along $\mathbf{m}$. This is because for such points the normal displacement of the plate faces turns to zero: $\hat{\mathbf{A}}_{S_n} \cdot \mathbf{n} = 0$. Hence, $\hat{v}_{S_n}(\omega^{(n)}) = v_l$ entails $v''_{S_n}(\omega^{(n)}) = 0$ and the tangency of the curves $v'_{S_n}(\omega)$ and $\hat{v}_{S_n}(\omega)$ at $\omega^{(n)}$, see Fig. 4.

In conclusion, it is noted that the low-frequency dispersion of the real part of S_0 branch has been studied for isotropic immersed plates in Ref. [23] with a purpose to emphasize inequality (32). The coefficient of the 'fluid-induced' dispersion B_{S_0} was inferred there by truncating the Taylor expansion in complex v after the first order. This is incorrect. The first-order variation of the real part $(v' - \hat{v})/\hat{v}$ is in fact of the same order as the omitted second-order term $(v''/\hat{v})^2$. As a result, the formula obtained for B_{S_0} in Ref. [23] differs from the correct expression (Eq. $(35)_2$ reduced to the case of isotropy) by missing the term $-3c_{12}^2/c_{22}^2 = -3(1 - 2c_{66}/c_{11})^2$ in the parentheses. Another oversight in Ref. [23] is that the 'fluid-induced' relative velocity difference $B_{S_0}(\rho_f/\rho)^2\left(\omega h/\hat{v}_{S_0}^{(0)}\right)^2$ equal to $[v'_{S_0}(\omega) - \hat{v}_{S_0}(\omega)]/\hat{v}_{S_0}(\omega)$ (see Eq. (30)) was attributed to $[v'_{S_0}(\omega) - \hat{v}_{S_0}^{(0)}]/\hat{v}_{S_0}^{(0)}$, i.e. referred to the origin *point* $\hat{v}_{S_0}^{(0)}$ $(= \hat{v}_{S_0}(0))$ rather than to the *branch* $\hat{v}_{S_0}(\omega)$. Such writing would mean that a positive $B_{S_0} > 0$ implies $v'_{S_0}(\omega) > \hat{v}_{S_0}^{(0)}$ (raising of $v'_{S_0}(\omega)$ above the $\hat{v}_{S_0}^{(0)}$ at any small ρ_f/ρ) instead of the correct consequence $v'_{S_0}(\omega) > \hat{v}_{S_0}(\omega)$.

4. Leaky waves near the thickness resonances

4.1. Preliminaries for an unloaded plate

Consider a free plate. The nth thickness resonance, associated with the αth bulk mode propagating along the normal $\mathbf{n}$ with the velocity c_α and the (unit) polarization $\mathbf{a}_\alpha$, occurs at the cutoff frequency

$$\omega_{\alpha,n} = \frac{\pi n}{2h} c_\alpha \quad (\alpha = 1, 2, 3;\ n = 1, 2, \ldots). \tag{38}$$

The (trace) velocity v becomes infinitely large with ω tending to $\omega_{\alpha,n}$, and hence its inverse, the slowness $s = v^{-1}$, is a more suitable parameter near thickness resonances. It is also convenient to adopt the 'local' branch labeling by the subscript (α, n) instead of j. In these terms, each cutoff frequency $\omega_{\alpha,n}$ gives rise to the slowness branch $\hat{s}_{\alpha,n}(\omega)$. It emerges from zero slowness and continues as a pure imaginary (non-propagating) branch on one side of $\omega_{\alpha,n}$ and as a real (propagating) branch on the other side of $\omega_\alpha^{(n)}$. Specifically, the real branch extends to the right or to the left $(\omega > \omega_\alpha^{(n)}$ or $\omega < \omega_\alpha^{(n)})$ if the in-plane group velocity $\mathbf{g}_{\alpha,n} \cdot \mathbf{m}$ along this branch is, respectively, positive or negative [7,24]. To link the further analysis to this pivotal point, consider for the moment the (real) frequency versus (real or imaginary) wavenumber dispersion branch $\hat{\omega}_{\alpha,n}(k)$ and its expansion at small $k = \omega s$ near the cutoff origin,

$$\hat{\omega}_{\alpha,n}(k) = \omega_{\alpha,n} + W_{\alpha,n}(2kh)^2 + \cdots. \tag{39}$$

Recall that $\mathrm{d}\hat{\omega}_{\alpha,n}/\mathrm{d}k = \mathbf{g}_{\alpha,n} \cdot \mathbf{m}$ for real k. By Eq. (39), the leading-order approximation of $\hat{s}_{\alpha,n}(\omega)$ near $\omega_{\alpha,n}$ is

$$\hat{s}_{\alpha,n}^2(\omega) = \frac{\omega - \omega_{\alpha,n}}{W_{\alpha,n}(2\omega_{\alpha,n}h)^2}, \tag{40}$$

implying that $\hat{s}_{\alpha,n}(\omega)$ is real for $\omega>\omega_{\alpha,n}$ and purely imaginary for $\omega<\omega_{\alpha,n}$ if $W_{\alpha,n}$ is positive, and vice versa if $W_{\alpha,n}$ is negative. For future references, let us write this relationship as

$$\operatorname{sgn} W_{\alpha,n}=\operatorname{sgn}(\mathbf{g}_{\alpha,n}\cdot\mathbf{m})_{\text{real }\hat{s}_{\alpha,n}}\quad\text{for }\Delta\omega=\omega-\omega_{\alpha,n}\to\begin{cases}+0 & \text{if } W_{\alpha,n}>0,\\ -0 & \text{if } W_{\alpha,n}<0.\end{cases}\tag{41}$$

The leading-order approximation (40) discarding the contribution $\sim(\Delta\omega)^2$ remains accurate within the cutoff vicinity restricted by the conditions

$$|\Delta\omega|\ll\omega_{\alpha,n};\ \ |\Delta\omega|\ll W_{\alpha,n}^2/W_{\text{next}},\tag{42}$$

where W_{next} is the coefficient in front of $(kh)^4$ in the next-order term in Eq. (39). Outside the range (42), the deviation of the slowness branch $\hat{s}_{\alpha,n}(\omega)$ from the leading-order estimate (40) is especially sizable in two cases. The first is when either real or imaginary extent of $\hat{s}_{\alpha,n}(\omega)$ near the cutoff has a folding point $\mathrm{d}\hat{s}_{\alpha,n}/\mathrm{d}\omega\to\infty$, which brings about a pair of complex-conjugated slowness branches. The second case occurs when there are two closely situated cutoffs, which give rise to the real-slowness branches with opposite signs of $\mathbf{g}_{\alpha,n}\cdot\mathbf{m}$. These curves move apart each other and, as a result, their imaginary extent curls into a small arch in between the cutoffs which rounds up the contrary trend of the real curves, see Refs. [7,10,11,24]. From the inverse viewpoint, it may be said that either of these two cases signals a small numerical value of the leading-order dispersion coefficient $W_{\alpha,n}$ relatively to the next one, and hence an 'early' violation of Eq. $(42)_2$ for a quite small $|\Delta\omega|$.

Analytical derivation of the coefficients of series (39) is of independent interest, which, however, exceeds the scope of the present paper. To avoid details pertaining to the general case of arbitrary anisotropy, we confine here to exemplifying $W_{\alpha,n}$ for the in-plane Lamb branches in an orthorhombic plate with the faces and the sagittal plane $(\mathbf{m},\mathbf{n})$ parallel to symmetry planes. Let the indices $\alpha=l,t$ correspond to the longitudinal and transverse modes, so that the cutoffs (38), related to these modes, are $\omega_{l,n}=\pi nc_l/2h$ and $\omega_{t,n}=\pi nc_t/2h$ with $c_l=\sqrt{c_{22}/\rho}$ and $c_t=\sqrt{c_{66}/\rho}$ ($X_1\|\mathbf{m}$, $X_2\|\mathbf{n}$). Then

$$\begin{aligned}W_{l,n}h&=\frac{1}{\pi n\sqrt{\rho c_{22}}}\left[\frac{c_{12}^2+c_{66}(c_{22}+2c_{12})}{4(c_{22}-c_{66})}-\frac{(-1)^n c_{66}^{3/2}(c_{12}+c_{22})^2}{\pi n\ \ c_{22}^{1/2}(c_{22}-c_{66})^2}\chi_{l,n}\right],\\ W_{t,n}h&=\frac{1}{\pi n\sqrt{\rho c_{66}}}\left[\frac{c_{11}}{4}-\frac{(c_{12}+c_{66})^2}{4(c_{22}-c_{66})}-\frac{(-1)^n c_{66}^{3/2}(c_{12}+c_{22})^2}{\pi n\ \ c_{22}^{1/2}(c_{22}-c_{66})^2}\chi_{t,n}\right],\end{aligned}\tag{43}$$

where

$$\chi_{l,n}=\begin{cases}\cot(\omega_{l,n}h/c_t) & \text{if } n \text{ is odd},\\ \tan(\omega_{l,n}h/c_t) & \text{if } n \text{ is even},\end{cases}\quad\chi_{t,n}=\begin{cases}\cot(\omega_{t,n}h/c_l) & \text{if } n \text{ is odd},\\ \tan(\omega_{t,n}h/c_l) & \text{if } n \text{ is even}.\end{cases}\tag{44}$$

Given that $\mathbf{m}$ is parallel to the axis of transverse isotropy, Eqs. (43) and (44) reduce to the result of Ref. [25].

Recall that the dispersion equation for a fluid-loaded plate involves the term $\Phi_{\text{plate}}\equiv Y_1^{(\mathbf{n})}\pm\sqrt{Y_2^{(\mathbf{n})}Y_2^{(\mathbf{n})*}}$, see Eq. (11). In the vicinity of the cutoff $\omega_{\alpha,n}$, within which the branch $\hat{s}_{\alpha,n}(\omega)$ has no folding points, the singular part of this term, considered as a function of s,ω and pre-multiplied by $-s^{-1}$, is

$$-\frac{1}{s}\Phi_{\text{plate}}(s,\omega)\propto\frac{2\widetilde{a}_{\alpha,n}(\omega)}{\rho\left[\hat{s}_{\alpha,n}^2(\omega)-s^2\right]},\tag{45}$$

where $\widetilde{a}_{\alpha,n}$ replaces $a_j/\hat{v}_j^3$ of Eq. (11). Note that, despite the similarity of $\mathbf{g}_{\alpha,n}\cdot\mathbf{m}=0$ and $\mathrm{d}\hat{s}_{\alpha,n}/\mathrm{d}\omega\to\infty$ at $\omega=\omega_{\alpha,n}$ to the case of folding points ($\mathbf{g}_j\cdot\mathbf{m}=0$, $\mathrm{d}\hat{v}_j/\mathrm{d}\omega\to\infty$ for a finite $\hat{v}_j$), $(\mathrm{d}\hat{s}_{\alpha,n}^2/\mathrm{d}\omega)_{\omega_{\alpha,n}}$ is well defined by Eq. (40) and the residue $\tilde{a}_{\alpha,n}(\omega)$ at the pole $\hat{s}_{\alpha,n}^2(\omega)$ is a locally analytical function of $\Delta\omega=\omega-\omega_{\alpha,n}$. Denote its expansion about $\omega_{\alpha,n}$ by

$$\widetilde{a}_{\alpha,n}(\omega)=\widetilde{a}_{\alpha,n}^{(0)}+\widetilde{a}_{\alpha,n}^{(1)}(\omega)+\ldots,\quad\text{where }\widetilde{a}_{\alpha,n}^{(0)}=\widetilde{a}_{\alpha,n}(\omega_{\alpha,n}),\ \widetilde{a}_{\alpha,n}^{(1)}(\omega)\sim\Delta\omega.\tag{46}$$

The leading-order term is

$$\tilde{a}^{(0)}_{\alpha,n} = \frac{(\mathbf{a}_\alpha \cdot \mathbf{n})^2}{2W_{\alpha,n}h(2\omega_{\alpha,n}h)^2}. \tag{47}$$

If the vertical direction $\mathbf{n}$ admits a purely transverse bulk mode ($\alpha = t$), then $\mathbf{a}_t \cdot \mathbf{n} = 0$ leads in the vicinity of the transverse cutoffs $\omega_{t,n}$ to

$$\tilde{a}^{(0)}_{t,n} = 0, \quad \tilde{a}^{(1)}_{t,n} = \frac{\omega - \omega_{t,n}}{2W^2_{t,n}h(2\omega_{t,n}h)^4} V^2_{t,n}, \tag{48}$$

where, for arbitrary anisotropy,

$$V_{t,n} = \sum_{\alpha=1,\alpha\neq t}^{3} (\mathbf{a}_\alpha \cdot \mathbf{n}) \frac{c_t^2 c_\alpha}{c_t^2 - c_\alpha^2} (\mathbf{a}_t \cdot \mathbf{N}_1 \mathbf{a}_\alpha + \mathbf{a}_\alpha \cdot \mathbf{N}_1 \mathbf{a}_t) \chi_{t,n}. \tag{49}$$

For the orthorhombic-plate setting introduced above, $W_{t,n}$ is given by Eq. $(43)_2$ and $V_{t,n}$ reduces to

$$V_{t,n} = \frac{c_{66}}{\sqrt{\rho c_{22}}} \frac{c_{12} + c_{22}}{c_{66} - c_{22}} \chi_{t,n}. \tag{50}$$

4.2. Dispersion equation for leaky waves near the cutoffs

Consider the leaky waves for a fluid-loaded plate in the vicinity of the free-plate cutoffs $\omega_{\alpha,n}$. The leaky-waves slowness $s_{\alpha,n}(\omega) = s'_{\alpha,n} + \mathrm{i}s''_{\alpha,n}$ is sought as a perturbation of the free-plate solution $\hat{s}_{\alpha,n}(\omega)$. In this context, two different types of thickness resonances are distinguished depending on the polarization $\mathbf{a}_\alpha$ of the resonant mode travelling along $\mathbf{n}$: the fluid-coupled resonances, for which $\mathbf{a}_\alpha$ is not purely transverse ($\mathbf{a}_\alpha \cdot \mathbf{n} \neq 0$, hence $s_{\alpha,n} \neq 0$ for $\omega = \omega_{\alpha,n}$), and the fluid-uncoupled, or transverse, resonances associated with the transverse mode ($\mathbf{a}_t \cdot \mathbf{n} = 0$, hence $s_{t,n} = 0$ for $\omega = \omega_{t,n}$).

The dispersion equation (16) with reference to Eqs. (45)–(48) can be approximated as follows:

$$\frac{2\tilde{a}^{(0)}_{\alpha,n}}{\rho\left[\hat{s}^2_{\alpha,n}(\omega) - s^2\right]} - \frac{\mathrm{i}}{\rho_f c_f} = 0 \tag{51}$$

in the vicinity of a fluid-coupled resonance $\omega_{\alpha,n}$, and

$$\frac{2\tilde{a}^{(1)}_{t,n}(\omega)}{\rho\left[\hat{s}^2_{t,n}(\omega) - s^2\right]} - \frac{\mathrm{i}}{\rho_f c_f} = 0 \tag{52}$$

in the vicinity of a fluid-uncoupled resonance $\omega_{t,n}$. Here the contribution $\sim(c_f s)^2$ is neglected in 'the fluid term', and the assumption of a small enough density ratio ρ_f/ρ allows approximating 'the plate term' to the leading order, which is valid in the frequency range $|\Delta\omega| = |\omega - \omega_{\alpha,n}|$ satisfying Eq. (42). For Eq. (52), it is also assumed that

$$|s^2 - \hat{s}^2_{t,n}(\omega)| \ll c_t \tilde{a}^{(1)}_{\alpha,n}(\omega). \tag{53}$$

A single-pole expansion used in Eqs. (51) and (52) is accurate insofar as the reference free-plate branch $\hat{s}_{\alpha,n}(\omega)$ is locally well detached from other branches. For instance, adjacent fluid-coupled and fluid-uncoupled resonances can be treated independently if the frequency gap between their cutoffs is much greater than the gauge value $2\rho_f c_f/\rho h$, otherwise the approximation validity depends on the local configuration of the free-plate slowness curves (see Section 4.4).

As discussed in Section 2.2, the formulation of the dispersion equation, which admits the leaky-wave solutions evolving from the free-plate ones, is unique. It defines the leaky wave, carrying energy away from the plate, as incorporating the modes that increase into the depth of loading fluids, if the in-plane group velocity $\mathbf{g}_{\alpha,n} \cdot \mathbf{m}$ of the reference free-plate solution is positive, and decrease, if $\mathbf{g}_{\alpha,n} \cdot \mathbf{m}$ is negative. In the vicinity of thickness resonances, however, this interpretation applies only to the real-valued extent of the reference

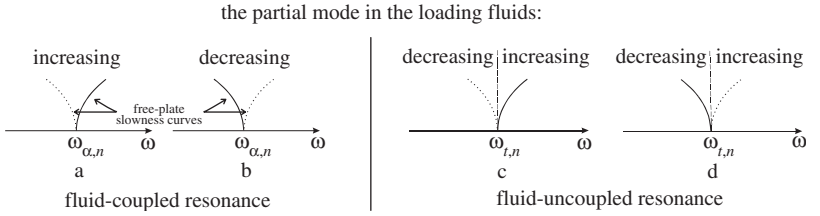

Fig. 5. The type of a partial mode, increasing or decreasing into the fluid half-space, that is incorporated by the leaky wave near the fluid-coupled and fluid-uncoupled thickness resonances with a positive or negative in-plane group velocity $\mathbf{g}_{\alpha,n}\cdot\mathbf{m}$ in the vicinity. The solid and dotted lines indicate, respectively, the real and pure imaginary extent of the free-plate slowness branch $\hat{s}_{\alpha,n}(\omega)$ near the reference cutoff $\omega_{\alpha,n}$ ($\alpha = t$ signifies the fluid-uncoupled resonance).

free-plate branches $\hat{s}_{\alpha,n}(\omega)$ (i.e., for $\omega\gtrless\omega_{\alpha,n}$ at $\mathbf{g}_{\alpha,n}\cdot\mathbf{m}\gtrless 0$), otherwise appealing to the group velocity is irrelevant. For the leaky wave, associated with the pure imaginary extent of $\hat{s}_{\alpha,n}(\omega)$, the link between the free-plate dispersion and the resulting type of fluid modes in the leaky wave is based on the observation that the sign of the imaginary part of slowness $s''_{\alpha,n}$, defined by Eq. (51) or (52) in the case of fluid-coupled or fluid-uncoupled resonances, coincides with the sign of $\widetilde{a}^{(0)}_{\alpha,n}$ or $\widetilde{a}^{(1)}_{t,n}(\omega)$, respectively. By Eqs. (47) and (48), this means that

$$\begin{aligned} \operatorname{sgn} s''_{\alpha,n} &= \operatorname{sgn} W_{\alpha,n} \quad && \text{if the resonance is fluid-coupled,}\\ \operatorname{sgn} s''_{t,n} &= \operatorname{sgn}(\omega-\omega_{t,n}) \quad && \text{if the resonance is fluid-uncoupled.}\end{aligned} \tag{54}$$

Recalling that positive or negative $s''_{\alpha,n}$ implies, respectively, decay or growth along $\mathbf{m}$ and hence increase or decrease into the fluids depth, relationship (54) in conjunction with Eq. (41) is illustrated in the form of a diagram in Fig. 5. The leaky wave near a fluid-coupled resonance involves the fluid modes of the same type and thus has the same trend along $\mathbf{m}$ on both sides of the cutoff frequency $\omega_{\alpha,n}$, which is obvious by continuity. Less trivial is the case of fluid-uncoupled (transverse) resonance: it is seen that the two interrelated attributes of the leaky wave—the type of fluid modes and the sign of leakage—must switch on passing the cutoff frequency $\omega_{t,n}$.

4.3. Leaky-wave slowness near the fluid-coupled and fluid-uncoupled resonances

Solving Eq. (51) with Eq. (47) yields the leading-order asymptotics for the slowness of the leaky wave near the cutoffs $\omega_{\alpha,n}$ of the fluid-coupled resonances,

$$\begin{aligned} [s'_{\alpha,n}(\omega)]^2 &= \frac{1}{2W_{\alpha,n}(2\omega_{\alpha,n}h)^2}\left[\Delta\omega+(\operatorname{sgn}W_{\alpha,n})\sqrt{(\Delta\omega)^2+\left(\frac{\rho_f}{\rho}\frac{c_f}{h}\right)^2(\mathbf{a}_\alpha\cdot\mathbf{n})^4}\right],\\ [s''_{\alpha,n}(\omega)]^2 &= \frac{1}{2W_{\alpha,n}(2\omega_{\alpha,n}h)^2}\left[-\Delta\omega+(\operatorname{sgn}W_{\alpha,n})\sqrt{(\Delta\omega)^2+\left(\frac{\rho_f}{\rho}\frac{c_f}{h}\right)^2(\mathbf{a}_\alpha\cdot\mathbf{n})^4}\right],\end{aligned} \tag{55}$$

where $\Delta\omega=\omega-\omega_{\alpha,n}$. The sign of $s''_{\alpha,n}(\omega)$ is determined by Eq. $(54)_1$. Neglecting the next-order terms is stipulated by small ρ_f/ρ and additionally fostered by a smallness of c_f relatively to the velocities of bulk modes in the plate material. By Eq. (55), the real part and the absolute value of the imaginary part of the leaky-wave slowness, taken to the leading order, cross each other at exactly the cutoff frequency:

$$s'_{\alpha,n}(\omega_{\alpha,n})\approx(\operatorname{sgn}W_{\alpha,n})s''_{\alpha,n}(\omega_{\alpha,n})\approx\sqrt{\frac{\rho_f}{\rho}\frac{c_f(\mathbf{a}_\alpha\cdot\mathbf{n})^2}{2|W_{\alpha,n}|h(2\omega_{\alpha,n}h)^2}}. \tag{56}$$

The difference between the exact values appears in the next order of approximation, so that $s'_{\alpha,n}(\omega_{\alpha,n})-|s''_{\alpha,n}(\omega_{\alpha,n})|\sim(\rho_f/\rho)^{3/2}$, and it is not sign-definite. Thus for small ρ_f/ρ the actual intersection of the curves $s'_{\alpha,n}(\omega)$ and $|s''_{\alpha,n}(\omega)|$ is only slightly shifted from $\omega_{\alpha,n}$ to the left- or right-hand side at a distance $|\Delta\omega|\sim(\rho_f/\rho)^2$.

Solving Eq. (51) with Eq. (48) gives the asymptotics for the vicinity of the fluid-uncoupled resonances $\omega_{t,n}$ as follows:

$$\left.\begin{aligned}[s'_{t,n}(\omega)]^2 &= \hat{s}^2_{t,n}(\omega)\left[1+\left(\frac{\rho_f c_f}{\rho\ h}\right)^2\frac{V^4_{t,n}}{4W^2_{t,n}(2\omega_{t,n}h)^4}\right]\\ [s''_{t,n}(\omega)]^2 &= \hat{s}^2_{t,n}(\omega)\left(\frac{\rho_f c_f}{\rho\ h}\right)^2\frac{V^4_{t,n}}{4W^2_{t,n}(2\omega_{t,n}h)^4}\end{aligned}\right\}\quad \text{for } W_{t,n}\Delta\omega>0,$$

$$\left.\begin{aligned}[s'_{t,n}(\omega)]^2 &= -\hat{s}^2_{t,n}(\omega)\left(\frac{\rho_f c_f}{\rho\ h}\right)^2\frac{V^4_{t,n}}{4W^2_{t,n}(2\omega_{t,n}h)^4}\\ [s''_{t,n}(\omega)]^2 &= -\hat{s}^2_{t,n}(\omega)\left[1+\left(\frac{\rho_f c_f}{\rho\ h}\right)^2\frac{V^4_{t,n}}{4W^2_{t,n}(2\omega_{t,n}h)^4}\right]\end{aligned}\right\}\quad \text{for } W_{t,n}\Delta\omega<0, \tag{57}$$

where $\hat{s}^2_{t,n}(\omega)=\Delta\omega/W_{t,n}(2\omega_{t,n}h)^2(\gtrless 0)$ by Eq. (40). The sign of $\Delta\omega=\omega-\omega_{t,n}$ determines the sign of $s''_{t,n}(\omega)$ according to Eq. $(54)_2$. Inserting Eq. (57) into Eq. (53) verifies the latter condition once $\rho_f c_f/\rho c_t$ is small, thereby confirming the consistency of approximation. By Eq. (57), the leaky-wave slowness, which is a perturbation of, specifically, the real extent of the free-plate branch, satisfies $s'_{t,n}-\hat{s}_{t,n}\sim(\rho_f/\rho)^2$ $(s'_{t,n}>\hat{s}_{t,n})$ and $|s''_{t,n}|\sim\rho_f/\rho$. In turn, the slowness, emerging from the imaginary extent $\hat{s}_{t,n}=\mathrm{i}\hat{s}''_{t,n}$, satisfies $s''_{t,n}-\hat{s}''_{t,n}\sim(\rho_f/\rho)^2$ $(|s''_{t,n}|>|\hat{s}''_{t,n}|)$and $s'_{t,n}\sim\rho_f/\rho$. It is noted that both local asymptotics (55) and (57) show an approximate symmetry between the curves of real and imaginary parts of the slowness about the cutoff frequency.

In conclusion, let us recall that a non-zero slowness related to the fluid-coupled resonance is a feature of the 'spatial leakage' (real ω and complex s), as opposed to the 'temporal leakage' (real s and complex ω). In the latter case, fluid loading keeps $s=0$ for any thickness resonance, but the cutoff frequency becomes complex [8,9,26,27]. If the plate faces are parallel to a symmetry plane, then the complex frequency of the longitudinal (fluid-coupled) resonances is given by the simple relation,

$$\omega_{l,n}=\frac{c_l}{2h}\left(\pi n-\mathrm{i}\ln\left|\frac{1+\rho_f c_f/\rho c_l}{1-\rho_f c_f/\rho c_l}\right|\right), \tag{58}$$

which is the same as for a fluid layer [28]. It is an exact evaluation for any ρ_f/ρ. By Eq. (58), fluid loading does not affect the real part $\omega'_{l,n}$ of the resonance frequency, which remains equal to the free-plate cutoff $\pi n c_l/2h$. It is, however, not so if the faces are not parallel to a symmetry plane and hence, generally, there is no pure longitudinal mode along $\mathbf{n}$. In this case, $\omega'_{\alpha,n}$ differs from $\pi n c_\alpha/2h$ in the measure of $(\rho_f/\rho)^2$.

4.4. Examples for light and heavy fluid loading

4.4.1. Light fluid loading

For the numerical illustrations of the light fluid loading, we take the same $(1\,\bar{1}\,0)$-cut copper plate, which has been used in the previous examples, but change the orientation of the propagation direction $\mathbf{m}$ to [1 0 0] (formerly it was $\mathbf{m}\|[1\,1\,0]$). The elastic coefficients of copper in the adopted reference basis with $X_1\|\mathbf{m}$ and $X_2\|\mathbf{n}$ are $c_{11}=170$, $c_{22}=222$, $c_{12}=123$, $c_{66}=75.5$ GPa. The reason for such a change is because the free-plate dispersion spectrum for this new geometry includes the branches with a negative group velocity near both fluid-coupled (longitudinal) and fluid-uncoupled (transverse) resonances, thus allowing us to test all possible options categorized in Fig. 5. The spectra for the free and water-loaded copper plate in the same frequency and slowness ($s<c_l^{-1}\approx 0.23\,\mu$s/mm) range are presented in Figs. 6a,b. For a clearer display, the real curves in Fig. 6a are not continued above the folding points (which give rise to complex branches); correspondingly the leaky-wave branch, emerging from the free-plate curve above the folding point, is omitted in Fig. 6b. A general discussion of the topological transformation, arising when the curve breaks apart at the folding point under the fluid loading, can be found in Refs. [10,11]. The focus of the present study is

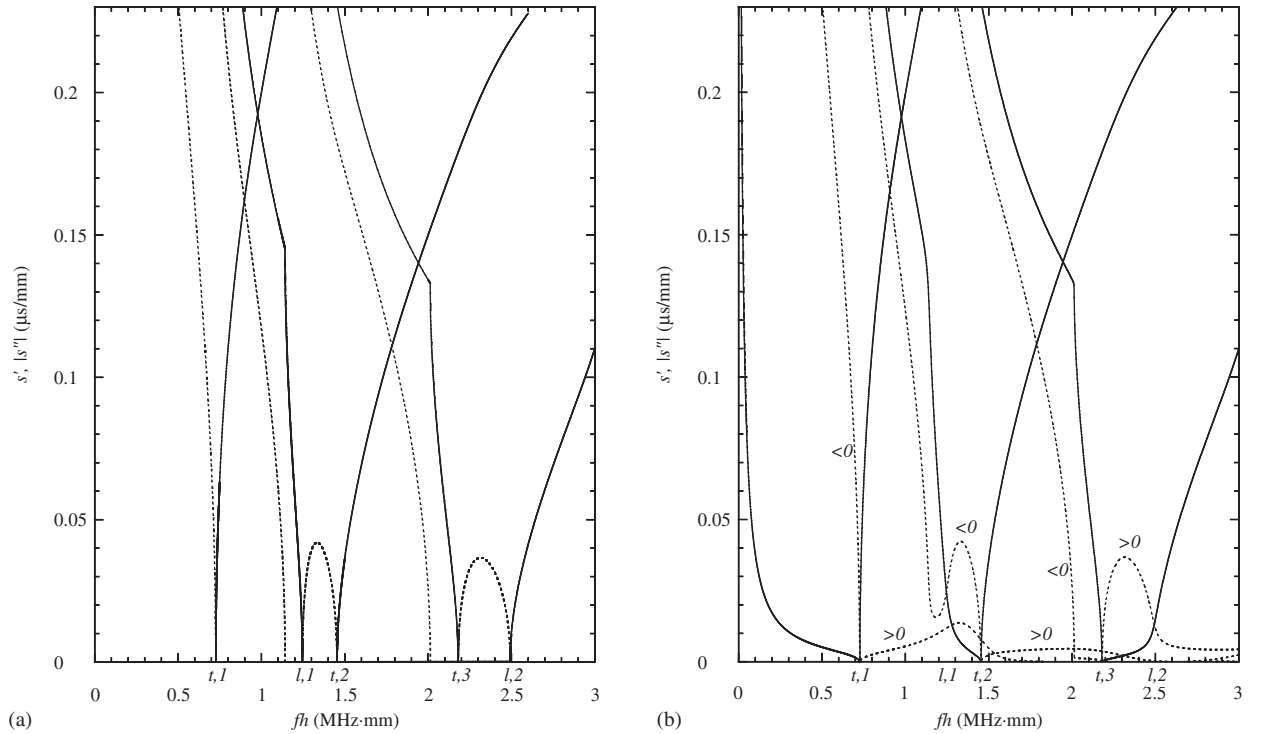

Fig. 6. Slowness curves $s(\omega)$, numerically calculated for the [1 0 0] propagation direction in a $(1\ \bar{1}\ 0)$-cut copper plate with free (a) and water loaded (b) faces. The reservations concerning the folding points are mentioned in the text. Solid and dotted lines show, respectively, the real and imaginary parts of slowness. Indicated in (b) are the signs of $s''(\omega)$ for leaky-wave solutions.

different—it seeks a quantitative evaluation of the spectral features specifically near the thickness resonances. Application of the near-cutoff asymptotics is demonstrated in Figs. 7a–c.

Fig. 7a displays a vicinity of the relatively well-detached first transverse resonance $t,1$ with the 'positive' dispersion trend (that is, $\mathbf{g}_{t,1}\cdot\mathbf{m}>0$ for $\omega>\omega_{t,1}$, case (c) in Fig. 5). Due to a small water-to-copper density ratio, the effect of fluid loading on the upper slowness branches is too slight to be captured at the scale of the figure, where these branches appear as a single line representing merged curves for a free and immersed plate. This applies both to the exact upper branches and to their analytical estimates by Eqs. (40) and $(57)_{1,4}$ for a free and immersed plate, respectively. Thus, the overall error of approximation basically resides in the free-plate asymptotics (40) truncated by the leading-order term. The immersed-plate asymptotics, however, come into play for the lower curves, $s'_{t,1}$ for $\omega<\omega_{t,1}$ and $s''_{t,1}$ for $\omega>\omega_{t,1}$, which emerge due to the fluid loading. Their zoom inserted in Fig. 7a confirms a good approximation by Eq. $(57)_{2,3}$.

The next Fig. 7b encloses the first longitudinal resonance $l,1$ with the locally 'negative' dispersion trend ($\mathbf{g}_{l,1}\cdot\mathbf{m}<0$ on its left-hand side, case (b) in Fig. 5) and the closely situated second transverse resonance $t,2$, which is of the 'positive' dispersion pattern. The presence of a folding point $\mathbf{g}_{l,1}\cdot\mathbf{m}=0$ on the real extent of the free-plate branch at $\omega<\omega_{l,1}$ and of a rapidly curling imaginary arch in between these two resonances inhibits the conditions, which stipulate the accuracy of asymptotics (see the comment to Eq. $(42)_2$). Therefore, the approximation rather quickly deteriorates on the left-hand side of the cutoff $\omega_{l,1}$ and in between $\omega_{l,1}$ and $\omega_{t,2}$. The accuracy is better on the right-hand side of $\omega_{t,2}$, where there is no folding points nearby. The same features pertain to the slowness curves near the neighbouring $t,3$ and $l,2$ resonances shown in Fig. 7c, except that now it is the transverse resonance, which has the locally 'negative' dispersion pattern, and it precedes the longitudinal resonance, which is of the 'positive' trend (respectively, cases (d) and (a) in Fig. 5).

Altogether, it is clear that the frequency range for a confident application of the leading-order asymptotics depends on local spectral features near a given resonance; however, once the basic assumption of a small density ratio ρ_f/ρ holds true, the approximation is reliable in the appropriately close proximity of any

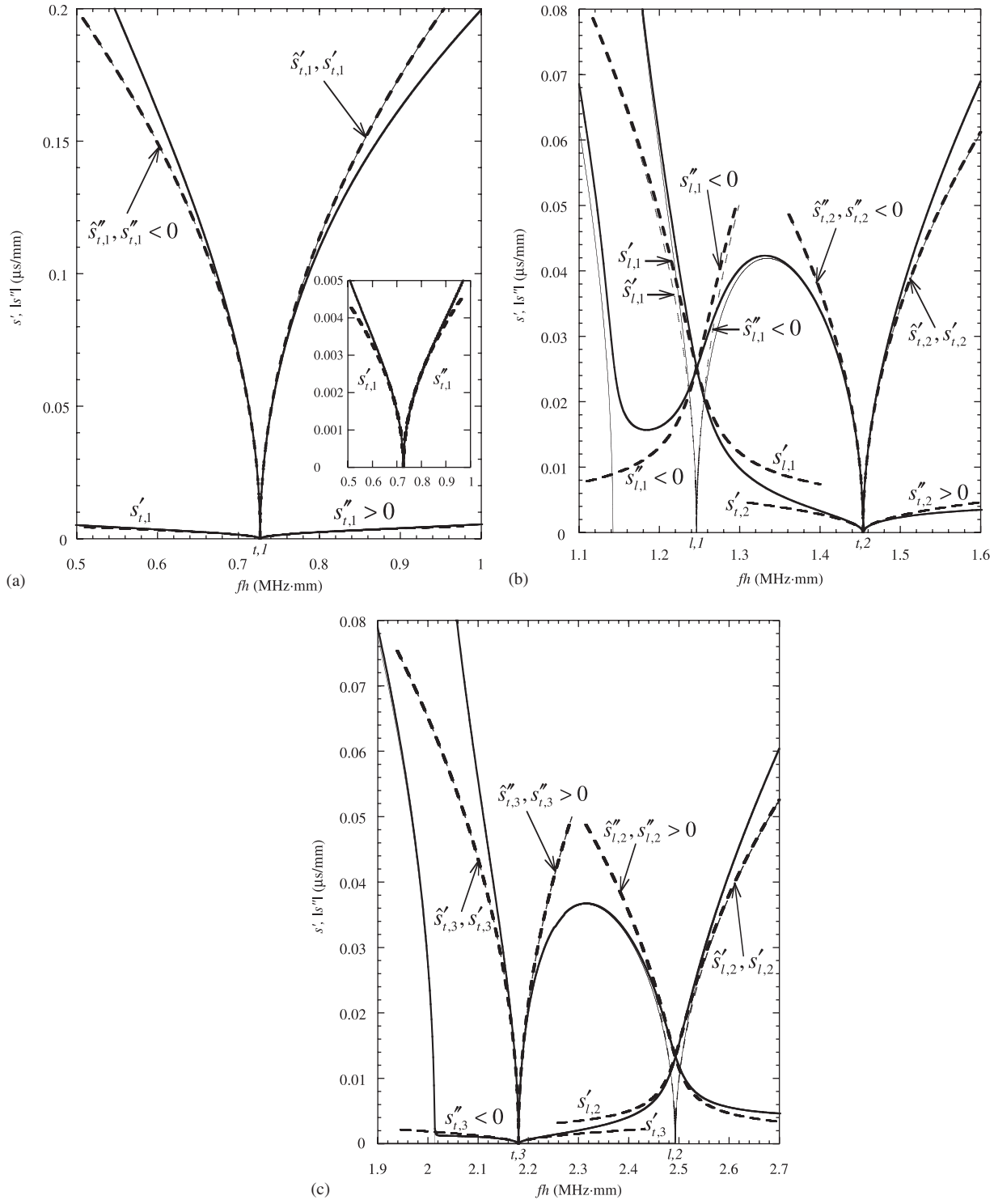

Fig. 7. A comparison between the exact slowness curves and their asymptotics near the thickness resonances displayed in Fig. 6b: (a) near $t,1$ (the inset zooms the lower curves); (b) near $l,1$ and $t,2$; (c) near $t,3$ and $l,2$. Solid bold and thin lines represent the exact numerical calculation for the immersed and free plate, respectively. The same display is used for real and imaginary parts. Dashed bold and thin lines show the asymptotics for the immersed (Eqs. (55) and (57) and free plate (Eq. (40)), respectively. The asymptotics are labelled by $s'_{\alpha,n}$, $s''_{\alpha,n}$ for the real and imaginary parts of the leaky-wave slowness, and by $\hat{s}'_{\alpha,n}$, $\hat{s}''_{\alpha,n}$ for the real and pure imaginary extent of the reference free-plate branches.

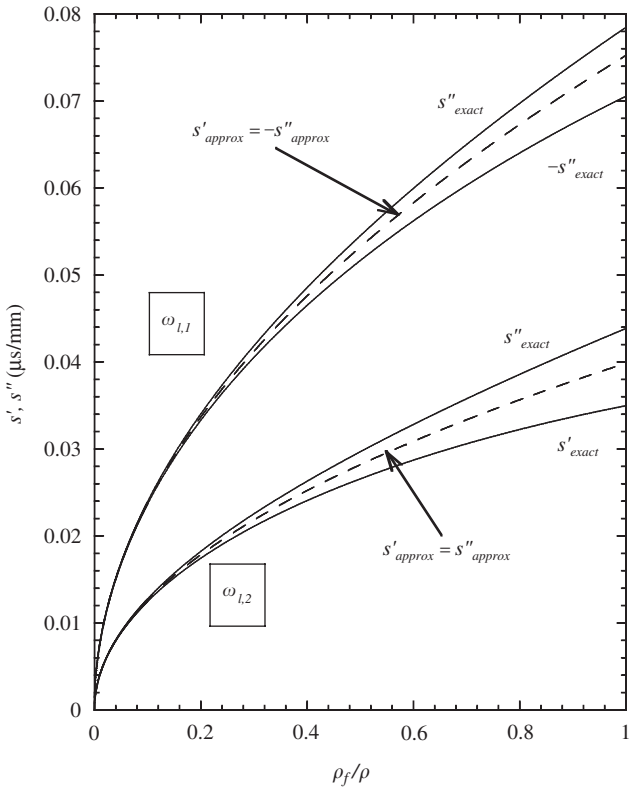

Fig. 8. The value of leaky-wave slowness at the frequency of a fluid-coupled resonance as a function of the loading-fluid density ($c_f = 1.5\,\mathrm{mm/\mu s}$ is fixed). The two first longitudinal resonances $l,1$ and $l,2$ for the [1 0 0] propagation direction in a $(1\ \bar{1}\ 0)$-cut copper plate are considered. The solid lines show the exact values of the real and imaginary parts $s'_{l,n}(\omega_{l,n})$, $s''_{l,n}(\omega_{l,n})$, dashed line represent their coinciding leading-order approximation by Eq. (56).

resonance. In particular, Eq. (56) furnishes a remarkably precise evaluation of the real and imaginary parts $s'_{\alpha,n}$ and $|s''_{\alpha,n}|$ at exactly the cutoff frequency $\omega_{\alpha,n}$ of a fluid-coupled resonance. Moreover, it turns out that the estimate given by Eq. (56) remains accurate enough even if ρ_f/ρ is actually not small, i.e. it is no longer a light fluid loading. This is borne out by the simulation presented in Fig. 8. Here the approximate values $s'_{l,n} = |s''_{l,n}|$, obtained from Eq. (56) for the cutoffs $\omega_{l,n}$ of two fluid-coupled resonances $l,1$ and $l,2$ in an immersed copper plate, are plotted as a function of ρ_f/ρ varying from 0 up to 1 (while the value of c_f is kept fixed). A comparison to the exact data (see the comment to Eq. (56)) confirms a reasonably good fit up to $\rho_f/\rho \lesssim 1$. At the same time, it is carefully noted that a successful estimation by Eq. (56) of the slowness value at exactly the cutoff frequency $\omega_{l,n}$ does not provide any evidence of an equally persisting validity of Eq. (55) for approximating a local *shape* of the slowness curves near $\omega_{l,n}$ under heavy fluid loading. This caveat is expanded in more detail below.

4.4.2. *Heavy fluid loading*

In order to explore the bounds of the asymptotics applicability, let us intentionally model an 'unfavourable' example. As such, we consider a Plexiglas plate in water. This case is 'awkward' for the two reasons: a relatively large density ratio $\rho_f/\rho = 1:1.18$ (which is aggravated by $c_f > c_t$, see the remark to Eq. (55)) and also an extremely close proximity of the cutoffs of longitudinal (fluid-coupled) and transverse (fluid-uncoupled) resonances. The consequences largely depend on the local spectral configuration.

The first pair of such neighbouring resonances, $t,2$ and $l,1$, is concerned in Fig. 9a, showing the range $\omega \geqslant \omega_{t,2}$ of principal interest. These resonances give rise to the free-plate slowness branches, whose real parts diverge from each other (extend into $\omega < \omega_{t,2}$ and $\omega > \omega_{l,1}$) and are connected by an imaginary arch within $\omega_{t,2} < \omega < \omega_{l,1}$. Such typical configuration [7,10,11,24], already encountered above for a copper plate

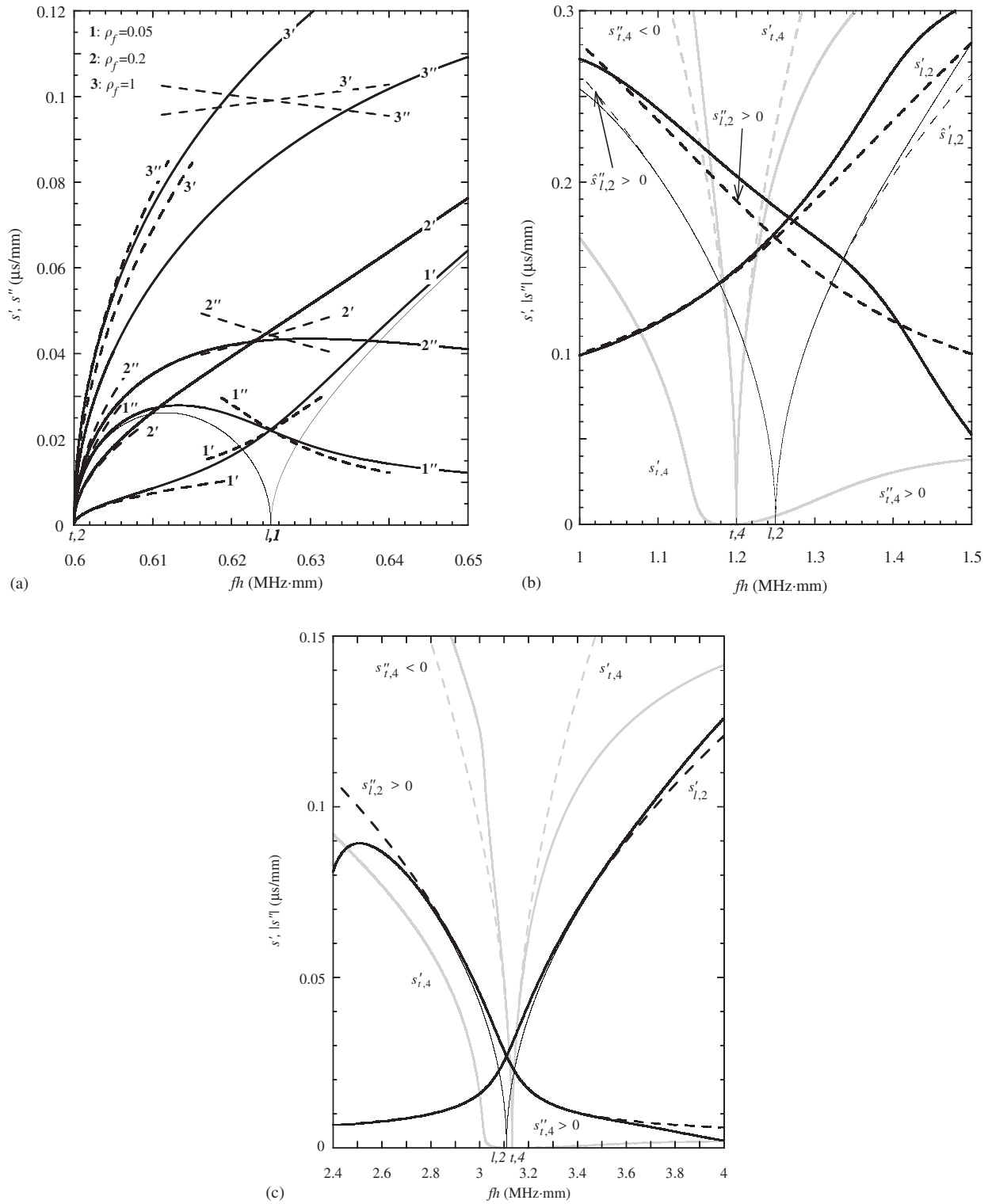

Fig. 9. Slowness curves near the thickness resonances under heavy fluid loading. (a) Plexiglas plate, spectral evolution near $t,2$ and $l,1$ resonances. The curves of the slowness real and imaginary parts for the three different values of ρ_f (indicated on the plot) are labelled, respectively, by $1',2',3'$ and $1'',2'',3''$; (b) water-loaded Plexiglas plate, the vicinity of $t,4$ and $l,2$ resonances; (c) water-loaded aluminium plate, the vicinity $l,2$ and $t,4$ resonances. In cases (b) and (c), the curves, associated with $t,4$ and $l,2$ resonances, are distinguished as grey and black, respectively. Other notations are the same as in Fig. 7: solid lines are the exact curves, bold for a fluid-loaded plate and thin for a free plate (added as a reference for the longitudinal resonances only); dashed lines are asymptotics (55) and (57).

(see Figs. 7b,c), may be said to be 'topologically interacting'. To illustrate its evolution to the case of heavy fluid loading, assume for the moment that the fluid density ρ_f varies from a fictitious small value up to that of water. The resulting sets of curves are displayed in Fig. 9a. Light fluid loading leads to a slightly disturbed pattern (the curves 1 in Fig. 9a), whose local shape near $\omega_{t,2}$ and $\omega_{l,1}$ is reasonably well approximated by Eqs. (57) and (55), respectively. The curves of the slowness real and imaginary parts intersect each other in the vicinity of $\omega_{l,1}$. On increasing ρ_f/ρ, the spectrum transforms so that this intersection point gradually shifts towards $\omega_{t,2}$ and, correspondingly, asymptotics (55) near $\omega_{l,1}$ becomes less adequate (the curves 2 in Fig. 9a). By the stage ρ_f/ρ reaches the water-to-Plexiglas value, the local spectrum (the curves 3 in Fig. 9a) has already been drastically modified relatively to its free-plate pattern: the exact branches $s'(\omega)$ and $s''(\omega)$ emerge from $\omega_{t,2}$ as monotonic curves satisfying $s'(\omega) \gtrless s''(\omega)$ for $\omega \lessgtr \omega_{t,2}$, which do not intersect at all and no longer show any evident impact of the $l,1$ resonance. As a result, Eq. (55), describing the curves near $\omega_{l,1}$ as a small perturbation about the free-plate pattern, is no longer relevant. What is, however, noteworthy is that Eq. (56), specifying Eq. (55) for exactly the cutoff point $\omega_{l,1}$, still provides a benchmark for the exact values $s'(\omega_{l,1})$ and $s''(\omega_{l,1})$. This state of affairs is to be borne in mind on interpreting Fig. 8, as noted on its discussion in Section 4.4.1.

Consider the next pair of closely situated fluid-uncoupled and fluid-coupled resonances, $t,4$ and $l,2$ (Fig. 9b). Unlike the previous pair, these ones give rise to the free-plate branches of a similar shape: for each of them, the real extent lies on the right-hand side of the cutoff and is continued by the imaginary extent with the same trend on the left-hand side of the cutoff. This local pattern may be referred to as 'topologically non-interacting'. In particular, there is no small round imaginary arch, which has connected two 'topologically interacting' cutoffs and molded a specific shape of the leakage curve $s''(\omega)$ under fluid loading. Now the leaky-wave slowness branches, associated with each of the nearby resonances, develop independently of each other. As a result, despite the heavy loading exerted by water on a Plexiglas plate, the two pairs of curves $s'_{t,4}(\omega)$, $s''_{t,4}(\omega)$ and $s'_{l,2}(\omega)$, $s''_{l,2}(\omega)$ stay independent (this is emphasized by the different colour of curves in Fig. 9b), by contrast to the 'aggregate' pair of the curves 3 in Fig. 9a. The curves $s'_{l,2}(\omega)$ and $s''_{l,2}(\omega)$ preserve a crossing point near $\omega_{l,2}$ and remain reasonably well approximated by their asymptotics (55). For the $t,4$ resonance, asymptotics $(57)_{1,4}$ for the upper curves, which only slightly differ from the free-plate branches, are also acceptable for a relatively large ρ_f/ρ in hand. On the other hand, asymptotics $(57)_{2,3}$ of the lower curves, emerging from zero due to fluid loading, fail fairly rapidly on moving away from the cutoff $\omega_{t,4}$, which is partly because this approximation (not displayed on Fig. 9b) is gauged against a very small reference value.

Fig. 9c shows one more example of a close pair of 'topologically non-interacting' longitudinal and transverse resonances affected by a 'rather heavy' fluid loading. It is represented by $l,2$ and $t,4$ resonances in a water-loaded aluminium plate ($\rho = 2.7\,\mathrm{g/cm^3}$, $c_l = 6.22\,\mathrm{mm/\mu s}$, $c_t = 3.133\,\mathrm{mm/\mu s}$). The asymptotics provide a reasonably good local approximation for the leaky-wave slowness.

5. Conclusions

The sextic plate formalism has been employed for analysing the leaky waves in anisotropic plates immersed in fluid. This formalism, which does not appeal to partial-mode decomposition, is especially efficient for an analytical treatment of the problem. With the dispersion equation written in terms of the plate admittance, the latter may be expanded near its poles $\hat{v}_j(\omega)$, which are the velocities for the unloaded plate. Seeking the leaky-wave velocity $v_j(\omega) = v'_j + \mathrm{i}v''_j$ (ω is real) as a perturbation about $\hat{v}_j(\omega)$ allows us to express the approximate solution via the residue of the plate admittance. The properties of the residue, which is proportional to the frequency derivative of $\hat{v}_j(\omega)$ and has the sign of the in-plane group velocity, are helpful for illuminating the basic features of the leaky-wave dispersion spectrum. Moreover, this approach provides explicit closed-form asymptotics for the leaky-wave velocity. Their derivation and analysis has been the main objective of the paper.

Usefulness of the low-frequency asymptotics for the upper fundamental branch(es) of leaky waves is enhanced by the fact that the small parameter in this case is a product of the fluid-to-solid density ratio ρ_f/ρ times the wavenumber-thickness variable kh. Hence the approximation is not restricted to light fluid loading. The leading-order estimate for the imaginary part of the fundamental branch is linear in $(\rho_f/\rho)kh$. The asymptotics for the real part shows that the shape of this curve transforms with growing ρ_f/ρ from the

downward trend to an upward. An explicit condition is given for the critical value of ρ_f/ρ, above which the trend of the curve becomes upward.

Special attention is given to the leaky-wave asymptotics near the thickness resonances. The same formalism is adapted to using the slowness $s = v^{-1}$ as a more suitable variable. The resonances are known to fall into two basic types with respect to fluid loading: fluid-coupled and fluid-uncoupled (associated with a transverse mode), for which, respectively, s', $s'' \neq 0$ and $s = 0$ at the cutoff frequency. This implies their different treatment. In particular, the choice of either increasing or decreasing fluid modes, incorporated by the leaky wave, is decided in the vicinity of a fluid-coupled resonance in a usual way, that is, by the sign of in-plane group velocity associated with the real extent of the reference free-plate branch. The link is less trivial in the case of a fluid-uncoupled resonance. It reads that the leaky-wave branch involves the decreasing fluid modes for ω on the left-hand side of the cutoff and the increasing fluid modes on the right-hand side of the cutoff for any fluid-uncoupled resonance, regardless of signs of the group velocity.

Efficiency of the asymptotics in the vicinity of the resonances certainly depends on the density ratio ρ_f/ρ, and also on the type of resonance and on the local configuration of the reference dispersion branches in the free-plate spectrum. Near the fluid-uncoupled resonances, the leaky-wave slowness, which evolves from the real and pure imaginary extents of the free-plate branch, differs from these only to the measure of $(\rho_f/\rho)^2$ (hence the accuracy of approximation basically resides in the free-plate asymptotics). In turn, the real and imaginary curves of leaky-wave slowness, which emerge near a fluid-uncoupled resonance from zero, are of the order of ρ_f/ρ. The case of fluid-coupled resonances is, naturally, more involved. Interestingly, the leading-order estimate of the leaky-wave slowness at exactly the cutoff frequency of a fluid-coupled resonance, giving the same value $\sim\sqrt{\rho_f/\rho}$ for both real and imaginary parts, maintains a good accuracy even when ρ_f/ρ is not small (heavy fluid loading). The asymptotics assume a leading-order expansion about an isolated pole. Their reliability in the case of two closely situated resonances largely depends on the local spectral topology. For the Lamb spectrum in an orthorhombic plate, the neighbouring resonances are the fluid-coupled and fluid-uncoupled ones. Provided that they are 'topologically interacting', which is when the real extents of the two free-plate slowness branches near their cutoffs have contrary dispersion trends due to the opposite signs of group velocity, the leaky-wave asymptotics are restricted to small ρ_f/ρ and narrow frequency band. If these neighbouring fluid-coupled and uncoupled resonances are 'topologically non-interacting', i.e. give rise to the free-plate branches with a similar dispersion trend, the local asymptotics provide a reasonably good approximation even for relatively heavy fluid loading.

Acknowledgements

A.L.S. acknowledges partial support from the Russian Foundation for Basic Research (grant 05-02-16666).

References

[1] A.H. Nayfeh, *Wave Propagation in Layered Anisotropic Media*, North-Holland, Amsterdam, 1995.
[2] D.E. Chimenti, Guided waves in plates and their use in material characterization, *Applied Mechanics Reviews* 50 (1997) 247–284.
[3] A.L. Shuvalov, O. Poncelet, M. Deschamps, Analysis of the dispersion spectrum for fluid-loaded anisotropic plates: flexural-type branches and real-valued loops, *Journal of Sound and Vibration* 290 (2006) 1175–1201.
[4] A.L. Shuvalov, On the theory of wave propagation in anisotropic elastic plates, *Proceedings of the Royal Society London A* 456 (2000) 2197–2222.
[5] A.L. Shuvalov, Theory of plane subsonic elastic waves in fluid-loaded anisotropic plates, *Proceedings of the Royal Society London A* 458 (2002) 1323–1352.
[6] A.L. Shuvalov, General relationships for guided acoustic waves in anisotropic plates, *Proceedings of the Royal Society London A* 460 (2004) 2671–2679.
[7] B.A. Auld, *Acoustic Fields and Waves in Solids*, Vol. 2, Krieger, Malabar, FL, 1990.
[8] O. Poncelet, M. Deschamps, Lamb waves generated by complex harmonic inhomogeneous plane waves, *Journal of the Acoustical Society of America* 102 (1997) 292–300.
[9] M. Deschamps, O. Poncelet, Transient Lamb waves: comparison between theory and experiment, *Journal of the Acoustical Society of America* 107 (2000) 3120–3130.
[10] S.I. Rokhlin, D.E. Chimenti, A.H. Nayfeh, On the topology of the complex wave spectrum in a fluid-coupled elastic layer, *Journal of the Acoustical Society of America* 85 (1989) 1074–1080.

[11] A. Freedman, Effects of fluid-loading on Lamb mode spectra, *Journal of the Acoustical Society of America* 99 (1996) 3488–3496.
[12] J. Lothe, D.M. Barnett, On the existence of surface-wave solutions for anisotropic half-spaces with free surface, *Journal of Applied Physics* 47 (1976) 428–433.
[13] V.I. Alshits, M. Deschamps, G.A. Maugin, Elastic waves in anisotropic plates: short-wavelength asymptotics of the dispersion branches $v_n(k)$, *Wave Motion* 37 (2003) 273–292.
[14] T.C.T. Ting, *Anisotropic Elasticity*, Oxford University Press, New York, Oxford, 1996.
[15] M.F.M. Osborne, S.D. Hart, Transmission, reflection, and guiding of an exponential pulse by a steel plate in water. I. Theory, *Journal of the Acoustical Society of America* 17 (1945) 1–18.
[16] D.M. Barnett, S.D. Gavazza, J. Lothe, Slip waves along the interface between two anisotropic elastic half-spaces in sliding contact, *Proceedings of the Royal Society London A* 415 (1988) 389–419.
[17] Y.B. Fu, A. Mielke, A new identity for the surface-impedance matrix and its application to the determination of surface-wave speeds, *Proceedings of the Royal Society London A* 458 (2002) 2523–2543.
[18] V.I. Alshits, A.N. Darinskii, A.L. Shuvalov, Resonant reflection and refraction of sound at a liquid–crystal interface, *Soviet Physics-Solid State* 34 (1992) 1337–1346.
[19] O. Poncelet, A.L. Shuvalov, J.D. Kaplunov, Approximation of the flexural velocity branch in plates, *International Journal of Solids and Structures*, accepted for the publication.
[20] A. Bernard, M.J.S. Lowe, M. Deschamps, Guided wave energy velocity in absorbing and nonabsorbing plates, *Journal of the Acoustical Society of America* 110 (2001) 186–196.
[21] M. Castaings, B. Hosten, Guided waves propagating in sandwich structures made of anisotropic, viscoelastic, composite materials, *Journal of the Acoustical Society of America* 113 (2003) 2622–2634.
[22] F. Simonetti, M.J.S. Lowe, On the meaning of Lamb mode nonpropagating branches, *Journal of the Acoustical Society of America* 118 (2005) 186–192.
[23] W. Hassan, P.B. Nagy, Why fluid loading has an opposite effect on the velocity of dilatational waves in thin plates and rods, *Journal of the Acoustical Society of America* 102 (1997) 3478–3483.
[24] R.D. Mindlin, Waves and vibrations in isotropic, elastic plates, in: J.N. Goodier, N. Hoff (Eds.), *Structural Mechanics*, Pergamon, New York, 1960, pp. 199–232.
[25] J.D. Kaplunov, L.Yu. Kossovich, G.A. Rogerson, Direct asymptotic integration of the equations of transversely isotropic elasticity for a plate near cut-off frequency, *Quarterly Journal of Mechanics and Applied Mathematics* 53 (2000) 323–341.
[26] G. Durinck, W. Thys, P. Rembert, J.L. Izbicki, Experimental observation on a frequency spectrum of a plate mode of a predominantly leaky nature, *Ultrasonics* 37 (1999) 373–376.
[27] O. Lenoir, J.M. Conoir, J.L. Izbicki, The complex phase gradient method applied to leaky Lamb waves, *Journal of the Acoustical Society of America* 112 (2002) 1335–1345.
[28] J.M. Conoir, Reflexion et transmission par une plaque fluide, in: N. Gespa (Ed.), *La Diffusion Acoustique*, Cedocar, Paris, 1987, pp. 105–132.